UNIVERSITÀ
DEGLI STUDI
DI PADOVA

Sede Amministrativa: Università degli Studi di Padova

Dipartimento di Istologia, Microbiologia e Biotecnologie Mediche

SCUOLA DI DOTTORATO DI RICERCA IN BIOSCIENZE

INDIRIZZO GENETICA

CICLO XXIII

EXPRESSION AND FUNCTIONAL ROLE OF EMILIN-3, A PECULIAR MEMBER OF THE EMILIN/MULTIMERIN FAMILY

Direttore della Scuola : Ch.mo Prof. Giuseppe Zanotti

Coordinatore d'indirizzo: Ch.mo Prof. Paolo Bonaldo

Supervisore :Ch.mo Prof. Paolo Bonaldo

Dottorando : Alvise Schiavinato

THESIS CONTENTS

ABSTRACT

Emilin-3 is a glycoprotein of the extracellular matrix belonging to a family of proteins that contain a characteristic N-terminal cystein-rich region, the EMI domain. Knockout mice for Emilin-1, the prototypic protein of the family, display hypertension and reduced diameter of blood vessels due to increased bioavailability of active TGF-β1 that reduces the proliferation rate of vascular smooth muscle cells. This finding is in agreement with the distribution of Emilin-1, which is mainly present in the cardiovascular system. *In vitro* studies demonstrated that Emilin-1 through its EMI domain acts as an extracellular inhibitor of TGF-β1 processing. At difference from other emilins/multimerins, Emilin-3 has a unique protein structure, lacking the C-terminal C1q domain. Emilin-3 has a peculiar pattern of expression, as revealed by our studies in mouse and zebrafish. The gene is not expressed in the cardiovascular system, while it is present in tissues playing key roles during the development. Emilin-3 mRNA is abundant in the tail bud, notochord and chordoneural hinge, in the subventricular zone of the midbrain, around the osteogenic mesenchyme and in the developing gonads. In the perspective of studying Emilin-3 properties and unveiling its function, in this PhD work I carried out different *in vitro* and *in vivo* studies. *In vitro* experiments provided new information about Emilin-3 biochemical properties, indicating that Emilin-3 has a particular affinity for extracellular matrix components in a process mediated by heparin or other heparin sulfate proteoglycans. Biochemical studies reported in this thesis showed the relative importance of EMI and gC1q domains in the self-assembly process of emilin proteins. Furthermore, evidences of interaction between Emilin-3 and Emilin-1 were obtained. Functional studies in the zebrafish model allowed investigating the function of Emilin-3 *in vivo*. Morpholino-mediated knockdown of Emilin-3 orthologue genes in zebrafish embryos revealed am essential role for Emilin-3 during notochord development. Moreover, Emilin-3 morphant embryos displayed also abnormal differentiation of muscle pioneers, a process governed by notochord-derived signals. In summary, the data reported in this thesis provide the first detailed characterization, with both structural and functional insights, of the extracellular glycoprotein Emilin-3.

ABSTRACT (Italiano)

Emilina-3 è una glicoproteina della matrice extracellulare appartenente ad una famiglia di proteine caratterizzate dalla presenza nella loro porzione N-terminale di un domino ricco di cisteine, il dominio EMI. Topi *knockout* per Emilina-1, la proteina capostipite di questa famiglia, presentano ipertensione arteriosa e una riduzione del calibro dei vasi sanguigni, alterazioni che sono state attribuite ad una disregolazione del *signaling* del TGF-β. Queste osservazioni sono in accordo con la distribuzione proteica di Emilina-1, che è abbondantemente presente a livello del sistema cardiovascolare. Esperimenti *in vitro* hanno dimostrato che Emilina-1, attraverso il suo dominio EMI, agisce come inibitore extracellulare della maturazione del precursore del TGF-β in citochina matura. Emilina-3 possiede una peculiare struttura proteica in quanto è priva del dominio gC1q al suo C-terminale, che è invece presente in tutte le altre Emiline/Multimerine. Inoltre Emilina-3 presenta anche un pattern di espressione unico, come dimostrato con i nostri studi di espressione in topo e zebrafish. Il gene infatti non è espresso nel sistema cardiovascolare come gli altri geni della famiglia, ma è espresso durante la vita embrionale in distretti importanti per i processi di sviluppo. Il messaggero di Emilina-3 è abbondante nel *tail bud*, nella cerniera cordoneurale, nella zona subventricolare del mesencefalo, nel pericondrio delle ossa lunghe in formazione e nei primordi delle gonadi. Con la finalità di studiare le caratteristiche e la funzione di Emilina-3, durante il mio ciclo di dottorato ho intrapreso diversi studi sia *in vitro* che *in* vivo. Esperimenti condotti *in vitro* hanno rivelato alcune nuove proprietà di Emilina-3. Prima di tutto hanno portato a scoprire che Emilina-3 possiede una notevole affinità per la matrice extracellulare e che questa affinità è mediata da legami ad eparan-solfati di matrice, e che Emilina-3 è in grado di legare l'eparina. Ho inoltre studiato l'importanza relativa dei domini gC1q e EMI nella formazione dei multimeri ad alto peso molecolare delle Emiline. Inoltre ho potuto descrivere come Emilina-3 interagisca con Emilina-1, dimostrando per la prima volta in modo preciso l'interazione tra due membri della famiglia delle Emiline/Multimerine. Infine, studi funzionali *in vivo* condotti nel modello animale *zebrafish* hanno permesso, attraverso esperimenti di *loss of function* genica di svelare un ruolo inaspettato degli ortologhi di Emilin-3 in zebrafish per il normale sviluppo della notocorda. Accanto ad una funzione strutturale, gli esperimenti condotti per questo lavoro di tesi hanno permesso di apprezzare anche un ruolo di Emilin-3 nel processo di differenziazione dei precursori muscolari, un processo guidato da segnali derivanti proprio dalla notocorda. In conclusione, gli esperimenti riportati in questa tesi rappresentano la prima descrizione della glicoproteina Emilina-3, sia dal punto di vista strutturale che funzionale.

INTRODUCTION

The extracellular matrix

An extracellular matrix (ECM) is present within mammalian embryos from the two-cell stage and is a component of the environment of all cell types, although the composition of the ECM and the spatial relationships between cells and ECM differ between tissues (Adams and Watt, 1993). The ECM is well known for its ability to provide structural support for organs and tissues, for organizing cell layers by means of basement membranes, and for individual cells as substrates for migration. The role of ECM in cell adhesion and signaling to cells through surface receptors such as integrins has received much attention (Hynes, 2002; Berrier and Yamada, 2007; Legate at al., 2009). More recently, mechanical characteristics of the matrix, such as stiffness and deformability, were also recognized to provide inputs for cell behavior (Discher et al., 2009; Geiger et al., 2009). Thus, ECM molecules play vital roles in the determination, differentiation, proliferation, survival, polarity, and migration of cells. ECM signals are arguably at least as important as soluble signals in governing these processes, and probably more so (Hynes, 2009). The vertebrate genomes has hundreds of different genes coding for ECM proteins. Many of these genes are ancient, such as those composing the basement membrane toolkit (type IV collagen, laminins, nidogen, perlecan, and type XV/XVIII collagens), which is found in most metazoa, and it can be argued that basement membranes were crucial to the evolution of metazoa (Whittaker et al., 2006). However, many vertebrate ECM proteins and genes evolved much more recently, during evolution of the deuterostome lineage, and that expansion includes not only elaboration of preexisting families (for example, laminins and collagens) but also novel proteins (e.g., fibronectins and tenascins). ECM proteins are large and complex, with multiple distinct domains, and are highly conserved among different taxa. Many ECM proteins have dozens of individually folded domains, but the functions of only few of these domains were elucidated in detail until now. The ECM provides the architectural framework for tissues, imparting specific physical properties necessary for tissue integrity as well as positional information required by cells. At the same time, this architectural framework serves to situate, concentrate, and sequester growth factor complexes. One long-standing hypothesis is that the ECM binds growth factors. Many growth factors (e.g., fibroblast growth factors and vascular endothelial growth factors) bind avidly to heparin and to heparan sulfate, a component of many ECM proteoglycans (PGs). Hence, a generally held view is that heparan sulfate PGs act as a sink or reservoir of growth factors and may assist in establishing stable gradients of growth factors bound to the ECM; such gradients of morphogens play vital roles in patterning developmental processes. It is also often proposed that growth factors can be released from the ECM by degradation of ECM proteins or of the glycosaminoglycan components of PGs. Furthermore, some growth factors actually bind to their signaling receptors with heparan sulfate as a cofactor. The binding of fibroblast growth factor to its receptor depends on an heparan sulfate chain binding simultaneously (Mohammadi et al., 2005), and transforming growth

factor–β (TGF-β) ligands bind first to integral membrane PGs that "present" these ligands during signaling (Shi and Massague, 2003); effectively they act as solid-phase ligands. There are also increasing examples of growth factors binding to ECM proteins themselves, without the involvement of glycosaminoglycans, supporting the notion that the presentation of growth factor signals by ECM proteins is an important part of ECM function. Another concept is that intrinsic domains within ECM proteins might act as ligands for canonical growth factor receptors. This suggestion arose from the observation that laminin contains multiple epithelial growth factor (EGF)-like domains, as do many ECM proteins (e.g., laminins, tenascins, thrombospondins, fibrillins), which might bind to EGF receptors and signal as solid phase ligands (Engel, 1989). EGF-like domains derived from laminin (Schenk et al., 2003) or tenascin (Krishnan et al., 2008) and presented as soluble ligands can bind to EGF receptor and modulate its signaling, and it is often hypothesized that fragments of ECM proteins can be released by proteolysis (for instance, by matrix metalloproteases) and act as soluble ligands, similar to the idea that matrix-bound growth factors can be released by ECM degradation. In both cases, the ECM acts as a reservoir of growth factors (bound or intrinsic), which can be released as soluble factors for binding their receptors. There is increasing evidence for specific, direct binding of growth factors to ECM proteins (Krishnan et al., 2008, Vaday et al., 2000). For instance, Drosophila collagen IV binds Dpp, a bone morphogenetic protein (BMP) homolog, and enhances its interactions with BMP receptors. This collagen-BMP interaction is crucial in regulating the dorsoventral axis and the number of germinal stem cells in the ovary, and both processes are dependent on gradients of Dpp. Collagen IV is a universal constituent of basement membranes, and the key Dpp-binding motif identified in the C-terminal domains of the two Drosophila collagen IV subunits is highly conserved across phyla, suggesting that this interaction may be important in other contexts (Wang et al., 2000). Another instructive example is collagen II, the major collagen of cartilage that, near its N terminus, contains a chordin-like VWC domain that binds TGF-β1 and BMP-2, two chondrogenic growth factors. The region of the mRNA transcript encoding the VWC domain undergoes alternative spliced, and the domain is included in the prechondrogenic mesoderm and early developing cartilage but is excluded in the mature cartilage (Zhu et al., 1999). The VWC or chordin domain is found in many ECM proteins and in known regulators of BMPs, and it typically acts as a negative regulator of their functions (Garcia Abreu et al., 2002). These examples illustrate the capacity of conserved elements of ECM proteins in the positive or negative regulation of the functions of diffusible morphogens of the BMP family. The regulation of TGF-β signaling by ECM proteins is one of the best characterized examples of this capacity.

Regulation of TGF–β signaling by the extracellular matrix

The three TGF-β isoforms in mammals — TGF-β1, TGF-β2 and TGF-β3 — are multifunctional and act in an autocrine, paracrine and sometimes endocrine manner to regulate diverse developmental processes and maintain tissue homeostasis in the adult. The bioavailability of active TGF-β is regulated at multiple levels, including secretion and interaction with ECM components, and each step in the activation pathway is under tight control (ten Dijke, 2007). Each of the precursors of TGF-β isoforms 1 to 3 is cleaved by a furin protease to originate mature TGF-β and its propeptide, known as latency-associated peptide (LAP). The LAP and TGF-β remain noncovalently associated in a complex called the small latency complex (SLC), and in this form, TGF-βs are inactive (Rifkin, 2005; , ten Dijke, 2007).

The SLC can covalently attach to the large latent TGF-β-binding protein (LTBP) to form the large latent complex (LLC) (Figure 1A; Saharinen et al., 1996). Most cell types secrete TGF-β as part of LLC, although some cells (such as the bone cell line UMR-106) secrete SLC (Dallas et al., 1994). Four different LTPBs have been identified, of which LTBP-1, LTBP-3 and, to a lesser degree, LTBP-4 covalently bind to LAPs of all three TGF-β isoforms (Saharinen and Keski-Oja, 2000). LTBPs contain multiple epidermal-growth factor (EGF)-like repeats and Cys-rich domains that are also found in fibrillins, which are extracellular proteins that are required for elastic fiber formation. The C-terminal region of LTBP-1 binds to the N-terminal region of fibrillin-1, linking LLC to elastic microfibrils (Isogai et al., 2002). After secretion, LLC binds to the ECM via the N-terminal domain of LTBP and this interaction is further supported by covalent transglutaminase-induced crosslinks. Antibodies to LTBP-1 and inhibitors of transglutaminase activity inhibit the activation of latent TGF-β, which demonstrates that localization of LTBP to the ECM is required for effective TGF-β activation (Nunes et al., 1997; Flaumenhaft et al., 1993).

LTBPs might have multiple functions: they target the latent TGF-β complex to specific sites, including structural components within the elastic fibres, where they may be stored for later use. This targeting is determined by binding to ECM components, such as fibronectin, via the variable N-terminal regions of LTBPs. In addition, LTPBs stabilize latent TGFβ complexes and regulate their activation at the cell surface (Rifkin, 2005). Important evidence for these roles comes from mouse models that are either deficient in *Ltbp3* or have a hypomorphic muta- tion in *Ltbp4*. These mice are viable but have multiple phenotypes that are related to decreased TGF-β signalling and defects in elastic fibres (Sterner-Kock et al., 2000; Dabovic et al., 2002). These results indicate an important role for LTBPs in connective tissue deposition and as a local regulator of TGF-β availability.

There are several mechanisms for TGF-β activation, including degradation of ECM proteins such as fibrillin or LTBPs. Activation can also occur by cleavage or

conformational change in LAP, exposing or releasing the TGF-βs to bind and activate their receptors (Chaudhry et al., 2007; Ge and Greenspan, 2006). Another ECM protein, thrombospondin (TSP)-1, can activate TGF-βs by binding and dissociating LAP or by activating metalloproteases; mice lacking TSP-1 develop pneumonia because of reduced levels of active TGF-β in their lungs (Lawler et al., 1998). Yet another mechanism for activation of TGF-βs involves αvβ6 and αvβ8 integrins, which bind to Arg-Gly-Asp (RGD) sequences in LAP1 and LAP3 (Sheppard, 2005). αvβ8 integrin appears to cooperate with metalloproteases to release TGF-b. However, αvβ6 integrin activates TGF-β without any requirement for proteolysis. Instead, αvβ6 binds to LAP and, in the presence of mechanical strain between the cells expressing the integrin and the ECM to which the SLC is attached, it deforms LAP to expose the associated TGF-β (Fig. 1A). The activated TGF- β is not released in soluble, diffusible form but appears to act only at short range, perhaps as a bound solid-phase ligand. Thus, the binding, the sequestration in latent form, and the subsequent activation of TGF-βs all intimately involve a variety of ECM proteins. The whole assembly acts like a regulated machine incorporating both negative and positive regulation. Incorporation of TGF-β into the matrix anchors and localizes the growth factor in a latent form, which can subsequently be locally activated by proteolysis or by mechanical strain. Mutations in various ECM proteins, integrins, and RGD sites in the LAPs confirm the relevance of these interactions *in vivo*.

Further analyses of LAPs, LTBPs, and fibrillins show that the TGF-β–LAP complex binds to LTBP-1 through a specific TGF-binding (TB) domain and adjacent EGF domains. TB domains, as well as hybrid domains (hybrids of TB and EGF domains), are unique to fibrillins and LTBPs, and there are several in each of those proteins, suggesting that they may be able to bind other BMP family members. Indeed, proBMP-7 can bind to fibrillin-1 in an N-terminal region containing a hybrid and a TB domain (Gregory et al., 2005). Furthermore, fibrillin-2 and BMP-7 mutations interact in causing syndactyly and polydactyly in mice (Arteaga-Solis, 2001), and a related human disease, congenital contractural arachnodactyly, arises from mutations in fibrillin-2 (Ramirez et a., 2007, 29). Prodomains of BMP-4, -7, -10 and of Growth and Differentiation Factor (GDF) -5 were also demonstrated to form stable complexes with their grow factors dimers and to mediate stable interactions with the fibrillin-1 and -2 proteins (Sengle et al., 2008). More recently, the prodomain of BMP-5 was also shown to bind fibrillin-1 and -2 and GDF-8 (myostatin) to form a complex with another ECM molecule, perlecan, through its prodomain (Sengle et al., 2010). Altogether, these findings show that the interactions of different ECM molecules with diverse TGF/BMP/GDF family members potentially target different signals to different locations.

The implications of ECM-based regulation of TGF-β function for human diseases have recently become very clear in the case of Marfan syndrome, a genetic disease resulting from mutations in the gene for fibrillin-1 (Ramirez and Dietz, 2009). Like many other genetic diseases whose target genes encode ECM proteins, this disease is associated with defective assembly of ECM components — in this case, the microfibrils of which fibrillins are components. The phenotype was originally attributed to mechanical consequences of these structural defects. However, the

known associations of fibrillins with LTBPs suggest that activation of TGF-β s might also play a role. In mouse models of Marfan syndrome activation of TGF-β is markedly increased, and many of the phenotypic consequences of mutations in fibrillin-1 can be ameliorated by TGF-β antagonists, an insight that already has clinical applications (Ramirez and Dietz, 2009).

Recently, the elastic fibers associated glycoprotein Emilin1 was linked to the extracellular regulation of TGF-β1 maturation (Zacchigna et al., 2006)

Emilin-1

Emilin-1, initially named gp115, was isolated from chicken aorta and found to be particularly abundant in that tissue (Bressan et al., 1983). Immunofluorescence studies confirmed that this protein is strongly expressed in blood vessels and revealed its presence in the connective tissue of a wide variety of organs (Colombatti *et al.*, 1985). At the ultrastructural level, the molecule was detected in elastic fibers, where it was located at the interface between the amorphous core and the coat of microfibrils (the name Emilin is an acronym assembled from Elastin Microfibrils Interface Located proteIN) (Bressan *et al.*, 1993). Emilin-1 appears in early stage of aorta development in association with a network of maturing microfibrils. Moreover, the process of elastic fibers formation is altered by anti-Emilin antibodies, suggesting that the protein may be involved in elastogenesis (Bressan *et al.*, 1993). The role of the protein in elastic fibers assembly was confirmed by disruption of the *Emilin1* gene in mice. *Emilin1* null mice have a normal development and are morphologically indistinguishable from wild-type littermates, but a closer examination shows alteration in elastic lamellae of elastic arteries and cellular defects in morphology and anchorage (Zanetti *et al.*, 2004). Emilin-1 presents a multimodular structure that includes: *i)* a C-terminal gC1q domain similar to those of type VIII and type X collagens and endowed with cell adhesion-promoting functions (Colombatti *et al.*, 2000); *ii)* a short uninterrupted collagenous stalk and a long α-helical domain with high probability for coiled-coil structure formation in the central part; *ii)* a unique cysteine-rich sequence of approximately 80 amino acids, the EMI domain, that follows the signal peptide and forms the N-teminal end of the mature molecule (Colombatti *et al.*, 2000). Studies on Emilin-1 have demonstrated that the gC1q domain is necessary for the formation of non-covalent homotrimers and acts as a nucleation centre for triple helix and multimers formation (Mongiat *et al.*, 2000). Moreover, it was demonstrated that Emilin-1, through its C1q domain, promotes adhesion of smooth muscle cells (Doliana *et al.*, 1999) by the interaction with integrin $\alpha_4\beta_1$ (Spessotto *et al.*, 2003).

Studies on *Emilin1* null mice have revealed at least two striking phenotypes. One concerns the cardiovascular system, in which the protein is expressed both during development (Braghetta *et al.*, 2004) and in the adult. *Emilin1* deficient mice exhibit generalized reduction of arterial diameter, increased peripheral resistance and systemic arterial hypertension (Zacchigna *et al.*, 2006). More recent studies

have shown that Emilin-1 is involved in the regulation of the growth and in the maintenance of the integrity of lymphatic vessels. Indeed, *Emilin1* deficiency results into hyperplasia and enlargement of lymphatic vessels and in a reduction of anchoring filaments (Danussi *et al.*, 2008). The lymphatic vessels of *Emilin1* null mice are functionally altered, leading to a mild lymphedema associated with inefficient lymph drainage and increased leakage. Recently, a proteomic approach aimed at identifying secreted proteins expressed during cartilage formation has found Emilin-1 as one of the more abundantly expressed ECM proteins, suggesting an important role for Emilin-1 in cartilage and bone development (Wilson et al., 2010).

The Emilin/Multimerin family

It was later realized that *Emilin1* is member of a larger group of genes, identified as the EDEN (EMI Domain ENdowed) superfamily, distinguished by the presence of the N-terminal EMI-domain (Doliana *et al.*, 2000; Braghetta *et al.*, 2004). The presence of cysteine-rich domains has been reported in various proteins, including several constituents of elastic fibers or protein associated with them. For instance, Fibrillin-1 contains at least five different types of cysteine-rich motifs (Sinha *et al.*, 1998). The EMI domain, however, is rather unique since it is characterized by seven cysteine residues while most of the cysteine-rich domains described to date contain either six or eight. Moreover, positions of cysteine residues in the EMI domain are conserved: distances between C1 and C2, C5 and C6, and C6 and C7 are absolutely conserved, whereas minimal gaps are present between C2, C3 and C4 (Doliana *et al.*, 2000). In mammals, the EDEN superfamily comprises seven members: Emilin-1, Emilin-2, Emilin-3, Multimerin-1, Multimerin-2, Emid1 and Emid2.

Emilins and Multimerins share a similar structural organization, with the EMI domain at their N-terminus, a long central region with high probability to form coiled-coil structures and a C-terminal gC1q domain (Fig. 2A) (Hayward et al., 1995; Christian et al., 2001). Emids are part of a separate family, being formed by the EMI domain followed by a long collagenous domain with some triple helix interruptions (Leimeister *et al.*, 2002). Emilin-3 is the only member ot the Emilin/Multimerin family lacking the gC1q domain (Doi et al., 2004). This domain has been shown to be important for Emilin-1 cell-adhesive properties and for partecipating in Emilin-1 self assembly (Colombatti et al., 2000, Mongiat al., 2000). Data banks mining and mRNA analysis showed that murine *Emilin3* is the only gene of the family that can undergo alternative splicing, generating two differently spliced mature mRNAs coding for two protein isoforms that were named Emilin-3L and Emilin-3S (P. Bonaldo and coll., unpublished data). Emilin-3S is a shorter form that lacks the first 141 bp of the fourth exon. At least three coiled-coil motifs are predicted in the C-terminal region of Emilin-3 (Fig. 3A,B).

High sequence similarity between Emilins was found in EMI and gC1q domains. In particular, bioinformatics analysis of human and murine EMI domains revealed an

average similarity of 60%. Moreover, the seven cysteines of EMI domains are located at highly conserved positions: although the total lengths of domains are variable between 71 to 79 aminoacids, the distances between cysteines are conserved. Only the second cysteine is shifted downstream of four residues in Multimerin-2, while it is absent in Multimerin-1 (Doliana *et al.*, 2000).

Analysis of the expression of Emilin/Multimerin genes during murine embryonic and postnatal development indicated that they are largely expressed in the cardiovascular system and in mesenchymal cells of various organs (Braghetta et al., 2002, 2004; Leimeister et al., 2002). These studies in mice showed that individual Emilin/Multimerin genes have distinct expression patterns, although their territories of expression appear largely overlapping and the possibility of functional redundancy and mutual compensation was proposed (Braghetta et al., 2004).

The in vivo biological function of mammalian Emilins/Multimerins remains largely unknown, as only the Emilin-1 knockout mice phenotype has been described (Zacchigna et al, 2006).

The Emilin/Multimerin family in zebrafish

Each mammalian Emilin/Multimerin gene - except *Multimerin1* - is present with two distinct paralogs in zebrafish, showing comparable degrees of sequence conservation with the corresponding human gene (Milanetto et al., 2008). The deduced amino acid sequences of the eight zebrafish emilin proteins indicate that their domain structure strictly resembles that of mammalian Emilin/Multimerin proteins. They all possess an EMI domain at the N-terminal end, followed by a long region with a high probability of forming coiled coil structures. Notably, the EMI domain of zebrafish Emilins contains seven conserved cysteine residues like in mammals, the only exception being Emilin-3a, which lacks the second cysteine. Similarly to their human and murine counterparts, the C- terminal portion has a different organization in the various zebrafish Emilins and ends with a gC1q domain. This domain is missing in Emilin-3a and -3b, in agreement with the structure of mammalian Emilin-3 (Fig. 2B). As observed also in the mouse, zebrafish Emilin genes are abundantly expressed in the cardiovascular system (Milanetto et al., 2008). Briefly, *emilin1a* and *emilin1b* have similar but not identical expression patterns during early zebrafish development. They are both expressed in the circulatory system of trunk and tail, particularly in the caudal vein. Both transcripts are found in the midbrain and sclera even with some differences. At 48 hpf *emilin1a* transcript is found in the pronephros while *emilin1b* is found in the heart and developing neurocranium. Both Emilin-2 paralogs display a prominent expression in the cardiovascular system throughout zebrafish development. At 24 hpf *emilin2a* is found in clusters of macrophages within the yolk as well as in the circulatory system and in the dermis of trunk and tail. At 48 hpf, besides expression in vascular structures, *emilin2a* transcripts become detectable in the heart at the level of atrium. Similarly to *emilin2a*,

expression of *emilin2b* transcript is abundant in the cardiovascular system but at the 15-somite stage *emilin2b* shows also a peculiar expression in few specific territories of the central nervous system. At later stages *emilin2b* expression is maintained only in the heart and in the circulatory system of the head. *mmrn2a* is expressed in the heart, in the caudal vein, in the posterior retina, in the most anterior part of the floor plate, and in the fin buds in 24 hpf embryos. At this stage, *mmrn2a* transcript is also detected in a region of the anterior gut where the intestinal bulb will form. At 48 hpf, *mmrn2a* is expressed in the circulatory system of the head, in the heart, in the anterior floor plate, and in the prospective intestinal bulb. At 22 hpf, *mmrn2b* is expressed in the heart, in the inner side of the otic vesicle, in the ependymal cells lining the ventricles of midbrain and hindbrain and in the most posterior somites. At 48 hpf, *mmrn2b* transcripts are found in the posterior somites and in the mesenchyme of pectoral fins.

The two zebrafish Emilin-3 orthologous genes display the most peculiar expression patterns during development, in agreement with the distinct protein structure of Emilin-3. At all examined stages of zebrafish development, *emilin3a* and *emilin3b* have a very similar pattern of expression, which never includes cardiovascular structures. This is a remarkable difference from the other Emilin/Multimerin genes, confirming the different role of this divergent Emilin family member. At early stages (5- to 15-somite), *emilin3a* is markedly expressed in the tail bud at the level of the notochord, with prominent labeling of an area corresponding to the chordoneural hinge, a structure containing a multipotent stem cell population. In 20-somite embryos, labeling for *emilin3a* in the notochord becomes stronger especially at the level of the trunk and tail regions. At 24 hpf, expression in the notochord decreases and becomes restricted to the most posterior region, where the floor plate, the chordoneural hinge, and the hypochord are also stained. At 48 hpf, expression in the notochord and floor plate disappears and emilin3a transcripts are found in the cartilage elements of branchial arches and craniofacial developing skeleton. The expression pattern of *emilin3b* is very similar to that of *emilin3a* (Figure 2C). It is noteworthy to remember here that *emilin3a* lacks the second cysteine in the EMI domain, the same that is also missing in mammalian Multimerin-1. The biological significance of this structural feature is yet unknown (Milanetto et al., 2008).

Structure and function of the notochord

The notochord is an embryonic midline structure common to all members of the *phylum* Chordata. In higher vertebrates, the notochord exists transiently and has at least two important functions. First, the notochord is positioned centrally in the embryo with respect to both the dorsal-ventral and left-right axes. Here, it produces secreted factors that signal to all surrounding tissues, providing position and fate information. In this role, the notochord is important for specifying ventral fates in the central nervous system, controlling aspects of left-right asymmetry, inducing pancreatic fates, regulating the arterial versus venous identity of the major axial blood vessels and specifying a variety of cell types in the developing

somites (Christ et al., 2004; Danos and Yost, 1995; Fouquet et al., 1997; Goldstein and Fishman, 1998; Lohr et al., 1997; Munsterberg and Lassar, 1995; Pourquie et al., 1993; Yamada et al., 1993; Yamada et al., 1991). Second, the notochord plays an important structural role. As a tissue, it is most closely related to cartilage and is likely to represent a primitive form of cartilage. Accordingly, the notochord serves as the axial skeleton of the embryo until other elements, such as the vertebrae, form. In some vertebrate clades, such as the *Agnatha* (lampreys), and in primitive fish, such as sturgeons, the notochord persists throughout life. In higher vertebrates, however, the notochord becomes ossified in regions of forming vertebrae and contributes to the centre of the intervertebral discs, the nucleus pulposus (Linsenmayer et al., 1986; Smits and Lefebvre, 2003; Swiderski and Solursh, 1992). In vertebrates, the notochord arises from the dorsal organiser. The first major transition is from dorsal organiser to chordamesoderm. During early gastrula stages, the chordamesoderm, which is the direct antecedent of the notochord, becomes morphologically and molecularly distinct from other mesoderm. Genetic screens in zebrafish have identified two loci, *floating head* (*flh*) and *bozozok*, as being essential for this transition to occur (Amacher and Kimmel, 1998; Fekany et al., 1999; Solnica-Krezel et al., 1996; Talbot et al., 1995). As development proceeds, chordamesoderm cells acquire a thick extracellular sheath and a vacuole. Osmotic pressure within the vacuole acts against the sheath, gives the notochord its characteristic rod-like appearance, and provides mechanical properties that are essential for the proper elongation of embryos and for the locomotion of invertebrate chordates and many vertebrate species (Adams et al., 1990). This transition, from chordamesoderm to mature notochord, requires a number of genes that have been identified in zebrafish genetic screens (Odenthal et al., 1996; Stemple et al., 1996). For example, *bozozok* mutant embryos lack a morphologically distinct shield, and both *bozozok* and *floating head* mutant embryos fail to form a notochord (Fekany et al., 1999; Talbot et al., 1995).

Consistent with its structural role in vertebrate development, the notochord shares many features with cartilage. It expresses many genes that are characteristic of cartilage, such as those that encode type II and type IX collagen, aggrecan, Sox9 and chondromodulin (Dietz et al., 1999; Domowicz et al., 1995; Ng et al., 1997; Sachdev et al., 2001; Zhao et al., 1997). There is, however, one clear difference between chondrogenesis and notochord formation. Chondrocytes normally secrete a highly hydrated ECM, which gives cartilage its main structural properties (Knudson and Knudson, 2001). By contrast, while notochord cells produce a thick basement membrane sheath, they retain hydrated materials in large vacuoles (Adams et al., 1990; Coutinho et al., 2004; Parsons et al., 2002). These vacuoles allow notochord cells to exert pressure against the sheath walls, which gives the notochord its structural properties (Adams et al., 1990). There may be a direct relationship between notochord and cartilage, in which cartilage has evolved to secrete certain materials; by rerouting those materials to an internal vacuole, notochord cells have co-opted some of the essential structural properties of cartilage to their needs. The ultimate fate of the notochord also emphasises the relatedness of notochord and cartilage. During endochondral bone formation, the type II collagen-rich ECM of cartilage is deposited with type X collagen, which signals the eventual replacement of cartilage by bone (Linsenmayer et al., 1986; Schmid et al., 1991). Similarly, during the development

of vertebrae, notochord that runs through the middle of each vertebra first expresses type X collagen and is then replaced by bone (Linsenmayer et al., 1986). Between the vertebrae, the notochord does not express type X collagen and is not replaced by bone, but becomes the centre of the intervertebral disc, the nucleus pulposus (Aszodi et al., 1998; Smits and Lefebvre, 2003). Thus, notochord can become ossified in a fashion similar to cartilage. Consistent with this view, in mutant mice that lack type II collagen, the notochord is not replaced by bone, presumably because the type II collagen network is required for proper deposition of type X collagen (Stemple, 2005). In zebrafish, the formation of the peri-notochordal basement membrane and vacuoles are each affected by two phenotypic classes of mutations. One class, originally found to affect both notochord and brain development, comprises the bashful, grumpy and sleepy loci. These loci have recently been found to encode zebrafish laminin α1 (*bashful*), laminin β1 (*grumpy*) and laminin γ1 (*sleepy*), which are constituents of the basement membrane (Parsons et al., 2002). The second class of mutations was originally found to affect notochord and melanophore development early in embryogenesis, eventually leading to catastrophic cell death throughout mutant embryos. This class comprises *sneezy*, *happy* and *dopey*, which encode, respectively, the α, β and γ chains of the coatomer complex, which is an important component of the secretory pathway and is essential for survival of all eukaryotic cells (Coutinho et al., 2004). More recently, lysyl oxidase enzymes were shown to play an essential role in notochord development (Gansner et al., 2007) and zebrafish mutant for the collagen VIII and fibrillin-2 genes have been identified for their alterations in the notochord structure (Gansner et al., 2008. Altogether these data entail an important role of several ECM components in the development and maintenance of the normal notochord structure.

AIM OF THE RESEARCH

The *in vivo* function of the Emilin/Multierin proteins is still largely unknown. Previous studies in mice have unveiled a role for Emilin-1 in the cardiovascular system homeostasis through the modulation of TGF-β growth factor activity (Zacchigna et al., 2006) and in lymphatic tissue (Danussi et al., 2008). No functional clues are available at the moment for other members of the family. This thesis is focused mainly in the characterization of Emilin-3, the last identified member among Emilin proteins. The first part of this work regards studies on gene and protein expression and structure. In the second part, some functional clues, obtained *in vivo* by taking advantage of the zebrafish model, will be presented.

MATERIALS AND METHODS

Animals

Procedures involving animals and their care were conducted according to institutional guidelines in compliance with national laws.

Fish were maintained in the zebrafish facility in the Department of Biology of the University of Padua, Italy. Embryos were grown at 28.5 °C under standard conditions and staged according to standard rules and procedures (http://ZFIN.org). The stage of the embryos was determined by morphological features.

RT-PCR

Total RNA from mouse embryos and different organs of newborn and adult mice was extracted with TRIzol Reagent (Invitrogen) as recommended by the manufacturer. After first strand cDNA synthesis using 1 μg total RNA and random hexanucleotides, amplification was carried out in 50 μl reaction mixtures containing 0.1–0.3 μg cDNA, 10 mM Tris–HCl pH 9.0, 50 mM KCl, 1.5 mM MgCl2, 0.1% Triton X-100, 0.2 mM dNTPs, 25 pmol of each primer and 2U *TaqI* polymerase (Promega). After 35 amplification cycles the reaction products were separated in 1% agarose gels. The following primers and conditions were used: *Emilin3,* 5'-CCC GTT ACA GCC TCT ACA CCA CC-3' (forward), 5'-CAG CCC ACG CAC CTC ATC TAA CA-3' (reverse), annealing temperature: 61°C, reaction products: 696bp (Emilin-3L) or 555bp (Emilin-3S). *eIF1A:* 5'-AAG AAG TCT GAA GGC CTA TG-3' (forward), 5'-CAG AGA ACT TGG AAT GTA GC-3' (reverse), annealing temperature: 58°C, reaction product: 170bp

In situ hibridization

In situ hybridization on whole mouse embryos and on sections was performed exactly as described (Braghetta et al., 2002) using a digoxigenin-labeled antisense riboprobe synthesized from murine Emilin-3 clones. Non-specific hybridization was evaluated with the sense riboprobe (not shown).

Wild type zebrafish were raised and maintained at approximately 28.5°C, under a 14 hr light/10 hr dark photo-period. To facilitate visualization of RNA during in situ hybridization, embryos were treated with 0.003% phenylthiourea (Sigma) to block pigment formation. Whole-mount in situ mRNA hybridization was carried out essentially as described in Thisse et al. (1993), using a 65°C overnight

hybridization step. Probes used were: *shh* (Krauss et al., 1993), *col2a1* (Yan et al., 1995), *ntl* (Schulte-Merker et al., 1994).

cDNA constructs

All the construct used in this thesis were cloned into the pCS2+ expression plasmid. Cloning of mouse Emilin1, and Emilin1ΔEMI in pCS2+ expression vector were previously described in Zacchigna et al., 2006. For Emilin3 constructs, total RNA from a C57/Bl6 mouse embryo of 12.5 day was extracted with the TRIzol reagent (Invitrogen). 1 µg of RNA was retro-transcripted with the SuperScriptT III First Strand Reverse Transcriptase System (Invitrogen) using oligo-dT primers. The resulting cDNA has been used for the amplification reaction with the Phusion High Fidelity Taq polimerase (Finnzymes) with the following primers using the conditions suggested by the manufacturers: 5'-AAA GAA TTC CGA GGG ACA GAG TGA CGA C-3' (forward), 5'-TTT TCT AGA GTT GGT GGG ATC TGC ACT TT-3' (reverse). The obtained products have been cloned into the TOPO® vector (Invitrogen) and then subcloned into pCS2+ using EcoRI and XbaI sites. Since Emilin3 cDNA has a single NdeI site that is lost in the shorter spliced form, this enzyme has been used for the screening of the two forms. For the generation of the Chd-Flag-Emilin3 construct (having the signal peptide of Chordin followed by a Flag epitope, a gift of Dr. S. Piccolo), an Emilin3 fragment generated by the digestion of the full lenght Emilin3 cDNA with XhoI and SnaBI has been cloned into the pCS2+ Chd-Flag plasmid. The Emilin-3ΔEMI construct contains the deletion of aminoacids 54-189. cDNA coding for aminoacids 1-54 was generated by PCR using the Emilin3 full length plasmid as template with SP6 as the forward primer and the following reverse primer with the insertion of a NdeI restriction site (underlined): 5'-TTT cat atg ctg gcc ccg ggc gca gc-3'. This fragment has been cloned into EcoRI-NdeI sites of the Emilin3 full lenght construct generating the deleted plasmid. The Emilin1ΔgC1q plasmid contains a deletion of aminoacids 861-1017. A PCR product obtained using the full length plasmid, SP6 and the following reverse primers: 5'-TTT TCC CTG CTC CCC TTG AGG AC-3' were cloned in the TOPO® vector (Invitrogen) and then subcloned into pCS2+ using XhoI/XbaI sites. All the plasmids have been sequenced before use.

Cell culture and transfections

HEK293T cells were cultivated in Dulbecco's Modified Eagle's Medium (DMEM) containing 4.5 g/L glucose, 25 mM Hepes, 2 mM L-Glutamine (Invitrogen) and supplemented with 10% fetal bovine serum (Invitrogen). Cells were maintained at 37°C in a humidified 5% CO_2 atmosphere. Where indicated, cells were treated with 50 µg/ml of solube heparin (Sigma). For western blot and immunoprecipitation experiments, approximately 7.5 x 10^5 Cells were plated at 50% confluence on 6-well plates an transfected with the indicated plasmids using the calcium phosphate method (Sambrook et al., 1989). Briefly, DNA dissolved in

250 mM $CaCl_2$ was added dropwise to an equal volume of 2x Hepes-buffered saline (HBS) (280 mM NaCl; 10 mM KCl; 1.5 mM Na2HPO4; 12 mM dextrose; 50 mM Hepes) with gentle mixing. Calcium phosphate-DNA coprecititates solution was added dropwise to the Petri dish and immediately mixed by swirling. The day after transfection the cells were washed, fed with serum-free medium, and cell lysate and conditioned medium were collected after 48 hrs. Cell extracts were prepeared with ice cold NP-40 lysis buffer (25 mM Tris pH 7.5, 150 mM NaCl, 2.5mM EDTA, 10% Glycerol, 1%NP40) supplemented with a protease inhibitors cocktail (Roche). For the extracellular matrix preparation (ECM), cells were lysed in the dish at 4°C with RIPA buffer (50mM NaCl,25mM Tris-HCI, pH 7.5, 0.5% NP-40, 0.5% sodium deoxycholate, 0.1% SDS, and protease inhibitors). The plates were then rinsed three times in cold RIPA buffer and the extracellular material remaining on the dishes after removal of the cellular components was extracted by scraping at 90°C in 2x Laemmli sample buffer.These fractions were designated ECM.

Western blot

Transfected HEK293T cells were collected in ice-cold NP-40 lysis buffer or RIPA buffer. Sample loading was normalized for differences of transfection efficiency on the basis of β-galactosidase activity and protein samples were resolved under reducing or non reducing conditions by SDS-PAGE in 4-12 or 3-8% NuPAGE® Bis-Tris gels (Invitrogen) and blotted onto polyvinylidene difluoride membranes (Millipore). The filters were blocked with 5% non-fat dry milk (Biorad) in TBS 1x (TBS 10x: 80 g Tris; 24.2 g NaCl in 1 liter)-0.1% Tween20 (TBS-T) buffer and then incubated with the primary antibodies. Following washes with TBS-T buffer, the membranes were incubated with horseradish peroxidase-linked secondary antibodies (Amersham Bioscience) and reacting bands revealed with SupersignalWest-pico and -dura HRP substrates (Pierce). Primary antibodies and dilutions used were: polyclonal guinea pig anti-Emilin-3 1:2000/3000; polyclonal rabbit anti-Emilin-3 1:3000; polyclonal rabbit anti-Emilin-1 1:1000 (a gift of prof. A. Colombatti), goat anti-LAP antibody (R&D systems), 1:1000; polyclonal rabbit anti-Flag 1:1000 (SIGMA). For agarose-acrylamide composite gels, the acrylamide solution (4 ml of 30% acrylamide solution + 12.5 ml of 1.5M Tris/HCl pH8.8, 0.4% SDS) was mixed with the agarose solution (0.25 g of pure agarose in 33 ml of water) after equilibration at 65°C; 90 µl of 10% ammonium persulfate and 38 µl of TEMED were added. Gels were let to harden at room temperature and then loaded with samples diluted in a loading buffer containing 0.4% SDS and 2M urea.

Immunoprecipitation

For immunoprecipitation experiments of transfected cells, cell lysates were prepeared with ice cold NP-40 or RIPA buffers with the addiction of fresh protease inhibitors. Conditioned media were clarified by brief centrifugation. For Flag-

mediated immunoprecipitation, 20 µl of anti-Flag M2 Affinity Gel (SIGMA) prepeared according to the manufacturer's instructions were used for each sample. The resin was washed 3 times in a solution of PBS, 1,5 mM $MgCl_2$ and 0,05% CHAPS. After 5 hrs of block in 2% BSA the resin was added on the samples and incubated in a roller shaker overnight at 4°C. The next day, samples were washed three times in NP-40 or RIPA buffer and the bound proteins were eluted with 35 µl of 2x sample buffer for 3 min at 90°C and analyzed by SDS-PAGE and immunoblotting. For the heparin binding assay, total lysates of transfected HEK293T cells were incubated overnight with 50 µl/sample of heparin-Sepharose beads or with unconjugated beads. The beads were washed with lysis buffer three times at room temperature, and the bound proteins were eluted with buffers with different NaCl concentrations. The presence of Emilin-3 proteins was examined by Western blot analysis. For immunoprecipitation of endogenous Emilin-3 proteins, E13.5 mouse embryos were pulverized by pestle and mortar and lysed in 5 volumes of extraction buffer (150 mM NaCl, 50 mM Tris/HCl pH 7,4, 2 mM EDTA, 1 % NP-40 with the addiction of protease inhibitors) for 30 min at 4°C. The homogenate was then centrifuged for 90 min with 12.000 g at 4°C. Half of the lysate was then pre-cleared with 50 µl of protein A-agarose beads overnight at 4°C on a rocking platform. The day after, extracts were collected from the beads after centrifugation and incubated with protein A-agarose beads conjugated with a rabbit pre-immune serum for 2 hrs at 4°C for two times. Finally cleared extracts were incubated overnight at 4°C in a rolling shaker with agarose beads conjugated with the rabbit Emilin-3 anti-serum. The day after, the beads were washed three times with cold extraction buffer and the immunoprecipitated proteins eluted in 2x sample buffer at 90°C for three minutes and analyzed by SDS-PAGE and immunoblotting with the guinea pig Emilin-3 antibody.

Deglycosylation experiment

Cell lysates and conditioned media from HEK293T cells transfected with the Emilin-3L construct were treated with different enzymes using the Enzymatic Protein deglycosylation kit E-*DEGLY* as recommended by the manufacturer. Reaction products have been analyzed by immunoblotting under reducing conditions using the same protocol as above.

Immunohistochemistry

Mouse tissues and E13.5 embryos were embedded in OCT (Sakura), snap-frozen, and stored at -80°C. Cryostatic sections (7 µm) were collected on positively charged slides (BDH SuperfrostPlus), air dried at room temperature and kept at -80°C. Before being used, the sections were equilibrated at room temperature and

hydrated with phosphate-buffered saline (PBS) and fixed for 5 min in methanol 100% at -20°C. Then, the sections were saturated with the blocking buffer (10% goat serum in PBS) for 30 min. Primary and secondary antibodies were diluted in 5% goat serum. The antibodies used were the following: polyclonal guinea pig anti-Emilin-3 (1:1000), polyclonal rabbit anti-Emilin-1 (1:250, kind gift of prof. A. Colombatti), polyclonal goat anti-β1-LAP (1:50, R&D Systems), polyclonal rabbit anti-Flag (1:1000, SIGMA); goat anti-rabbit IgG Cy3-conjugated antibody (Jackson Immuno Research); goat anti-rabbit IgG Cy2-conjugated antibody (Jackson Immuno Research); donkey anti-guinea pig IgG Cy-2 conjugated antibody (Jackson Immuno Research), donkey anti-goat IgG Cy-3 conjugated antibody (Jackson Immuno Research). The sections were saturated with the blocking buffer (10% goat or donkey serum in PBS) for 30 min and then incubated overnight at 4°C with the primary antibody. After three washes in PBS, secondary antibody was applied for 1 hr at room temperature. Nuclei were visualized with Hoechst or propidium iodide staining. The slides were mounted in 80% glycerol in PBS and observed in a Zeiss Axioplan microscope equipped with epifluorescence optics or in a Bio-Rad confocal microscope. For immunofluorescence in HEK293T, cells were plated on a boro-silicate glass coverslip in 24-well plate, after 48 hpf from transfection cells were washed two time in PBS, fixed in methanol/acetone for 5 min at - 20°C and processed as above.

For whole mount zebrafish immunofluorescence stainings, 24 and 48 hpf embryos were fixed for two hours at room temperature in 4% PFA, dehydrated in methanol and stored in 100% methanol at -20°C. The day of the experiment, embryos were incubated for 7 min in acetone at -20°C, washed three times in PBT (PBS + 1% Triton) and then incubated in PBT with 10% goat serum for two hours at room temperature. Embryos were then incubated overnight with the primary antibodies in the same solution. The next day, after extensive washes, embryos were incubated for three hours at room temperature with the secondary antibodies. Embryos were washed extensively in the dark, with Hoechst or propidium iodide added at 1/1000 to one wash, then mounted for analysis. The primary antibodies used were the following: polyclonal rabbit anti-Emilin-3 (1:500), monoclonal mouse anti-Collagen II (1:250, DSHB), monoclonal mouse anti-fast myosin light chains 1f and 3f (1:1000, DSHB), monoclonal mouse anti-Engrailed/invected (1:10, DSHB). All embryos were mounted in 1.5 % low melting agarose and images were acquired with a Bio-Rad confocal microscope.

Morpholino injection

Morpholino oligonucleotides (Nasevicius and Ekker, 2000) targeting splicing sites and starting codons of *emilin3a* and *emilin3b* were resuspended in Danieau buffer, diluted to include 0.05% phenol red, and injected into one- to four-cell embryos at the indicated concentrations. A standard control morpholino (Gene Tools, LLC) was likewise prepared and injected. Morpholino sequences are as follows:

emilin3a splice: 5'- TTA CTC ATG GAT ACT TAC TTG TGC C -3'; emilin3b splice: 5'- TAG CGT TTA CTT ACT TAT GAT GCC C -3'; emilin3a start: 5'- TGC AAA ATC TTC TCC AGT AGC ATG A-3'; emilin3b start: 5'- ACG GAA ATG CAA GAA TCC ACC TCA T-3'; standard control: 5'- CCT CTT ACC TCA GTT ACA ATT TAT A-3'. Splice-blocking morpholinos efficacy was tested by RT-PCR of RNA collected from 24 hpf wilde type, control and morphant embryos using the following primers: emilin3a, 5'-TAC GTG CTG AAA TTG GTG GA -3' (forward); 5'-GGA ACA GCT TGA CCT TCG AG-3'(reverse); emilin3b 5'-ACT CAA GCA AGC TGG ACC AT-3' (forward); 5'-CCT TGT GTA GTG GAG CGA CA-3' (reverse).

Transmission Electron Microscopy

Dechorionated embryos were fixed in 2.5% glutaraldehyde/0.1 M sodium cacodylate and sequentially stained with osmium tetroxide and uranyl acetate. They were then dehydrated, embedded in PolyBed 812, and thin sectioned on a Reichert-Jung Ultra-Cut. Slices were post- stained in 4% uranyl acetate and lead citrate, and viewed on a Zeiss 902 electron microscope. Photographs were recorded with Kodak EM film. Semithin sections were also stained with toludine blue for histologic analysys.

Pharmacologic treatments

Pharmacologic compounds were purchased from Sigma (St. Louis, MO). β-aminopropionitrile (A3134) SB431542 were prepared as 100 mM and 10mM stocks in egg water and dimethyl sulfoxide, respectively, and diluted in egg water. Embryos were incubated in compound starting at 3 hpf for βAPN and from 8 hpf for SB431542 and examined at 24 and 30 hpf. Images of representative fish mounted in 2% methylcellulose were acquired with a Leica DMR compound/Nomarski microscope equipped with a Leica DC500 digital camera.

RESULTS

Emilin-1 binds covalently proTGF-ß1 through LAP cysteine-33

To test the intriguing hypotesis the Emilin-1 could directly bind proTGF-β1, HEK293T cells have been transiently transfected with constructs coding for the two proteins. Conditioned media were then analyzed by immunoblotting under non reducing conditions. As shown in figure 4, while proTGF-β1 alone under non reducing conditions migrates as a dimer, when Emilin-1 was added to the system, a high molecular weight product appeared in the gel (Fig. 4A), suggesting the idea that Emilin-1 and proTGF-β1 formed a complex of high molecular weight. To validate this finding, conditioned media were immunoprecipitated for Emilin-1 using an anti-Flag antibody and samples were probed with anti β1-LAP antibody. Strikingly, β1-LAP was efficiently immunoprecipitated by Emilin-1 and migrated, under non-reducing conditions, at a molecular weight (more than 500 kDa) that suggested the formation of a complex between Emilin-1 homotrimers and β1-LAP dimers (Fig. 4B). It is known that the cysteine-33 of the β1-LAP is necessary for proTGF-β1 binding with LTBPs proteins (Saharinen et al., 1996, Fig 1B). When a plasmid coding for a proTGF-β1 with a mutated Cys-33 was co-transfected with Emilin-1, no LAP could be immunoprcipitated anymore, indicating that this cysteine is essential also for proTGF-β1/Emilin-1 interaction. Furthermore, as previously observed for LTBP proteins (Kantola et al., 2010), the co-expression with proTGF-β1 seemed to increase the amount of secreted Emilin-1 in the medium. Since it has been proposed that Emilin-1 interacts with proTGF-β1 through its EMI domain (Zacchigna et al., 2006), an Emilin-1 construct lacking the EMI domain was tested in the same experimental system. Even in this case, proTGF-β1 was immunoprecipitated and co-migrated with Emilin-1 trimers (Fig. 4C), indicating that cysteines of the EMI domain are not necessary for the interaction.

Emilin3 expression during mouse embryogenesis

Emilin3 mRNA expression was detected by RT-PCR in pre-implantation embryos and undifferentiated embryonic stem cells (data not shown). During post-implantation development, *Emilin3* transcripts were present at all studied stages with a peak of expression between E13.5 and E14.5. As reported for other Emilin genes, *Emilin3* expression decreases in all tissues after birth. In adult mice, *Emilin3* mRNA was detectable only in few of the examined tissues, namely testis, eye and brain (Fig. 5A,B).

Emilin3 expression during mouse embryogenesis was analyzed in details by *in situ* hybridization on whole-mount preparations at E8.5 and E9.5 and in serial sections of embryos from E10.5 to E14.5. At E8.5 *Emilin3* was expressed only in the region of the tail bud, while at E9.5 the tailbud and the primitive hindgut were both stained (Fig. 5C). At E10.5 a strong expression was detected in the esophageal bud, brachial arches, tail bud and a small region of the developing midbrain (data not shown). The expression in the midbrain, confined to the ventricular zone of the third ventricle, was still present at E11.5 (Fig. 6A-C) and E12.5, and disappeared around E13.5. It is interesting to note that the ventricular zone is a special region of the developing brain where neuronal precursor cells proliferate and differentiate. In particular, the ventricular zone of the ventral midbrain, where *Emilin3* mRNA is expressed, is involved in the differentiation of dopaminergic neurons, a process known to require the induction by Sonic Hedgehog and TGF-β family members (Wang, et al. 1995). Moreover *Emilin3* was strongly expressed throughout the developing gastrointestinal tract. While at early stages the mRNA was diffusely present in the wall of the gastro-intestinal system from the esophagus to the hindgut, later on its distribution became restricted to a thin layer that corrisponds to the myoenteric plexus, with a cranio-caudal gradient with the strongest signal in the esophagus (Fig. 6F-H). Gonadal ridges were also strongly expressing *Emilin3* throughout their development, while metanephric tissues and kidneys were almost negative. Expression of *Emilin3* mRNA was also detected in the intervertebral discs, in the region surrounding the main alveolar branches, in the subepidermal mesenchyme of the trunk, in the vibrissae, in the diaphgram and in the cephalic mesenchyme, a tissue originating from neural crests (Fig. 6A,I-Q). A strong expression was also detectable in the perichondrium around sites of bone and cartilage formation of trunk, skull and limbs (Fig. 6R). It is noteworthy that, while *Emilin3* was found to be expressed by cells of the perichondrium were mesenchymal cells condensate and can differentiate in osteoblasts, no *Emilin3* expression was detected in committed cells. Finally, it is interesting to note here that no *Emilin3* expression was found at any developmental stage in the embryonic cardiovascular system (except for a transient expression in the pericardium, results not shown), where, on the other hand, all the other Emilin genes were found to be abundantly expressed throughout the development (Braghetta, et al. 2002 and 2003).

Cloning and expression of murine Emilin3 cDNAs

In order to transfect murine full-length *Emilin3* cDNAs in eukaryotic cells, the alternatively spliced *Emilin3* transcripts coding for the two different protein isoforms (Emilin-3L and Emilin-3S) were amplified by RT-PCR from total RNA derived from E12.5 C57/BL6 embryos, cloned into pCS2+ expression vector and sequenced. Emilin-3L, Emilin-3S and the empty pCS2+ plasmid were transiently transfected in HEK293T cells using the calcium phosphate procedure, and cell extracts and conditioned media were collected and analyzed by western blot. Under reducing conditions, Emilin-3L and Emilin-3S migrated at about 105 kDa and 95 kDa respectively. Under non reducing conditions, instead, the two proteins

migrated at much higher molecular weights (about 270-320 kDa), with a size consistent with trimer formation (Fig. 7A). Despite the noticeable amounts of transfected protein detected in cell extracts, almost no protein could be detected in the conditioned media. To further investigate this finding, HEK293T cells were transfected with expression constructs coding for either Emilin-1, Emilin-2, or Emilin-3 proteins fused to a Flag epitope and a optimized signal peptide derived from the chordin protein (a gift of Dr. S. Piccolo), and cell lysates and conditioned media analyzed by western blot with an anti-Flag antibody. While both Emilin-1 and Emilin-2 proteins were present in both cell extract and medium samples, Emilin-3 was abundant in the cell extract but could not be detected in the conditioned medium (Fig. 7B). Therefore, absence of Emilin-3 in the conditioned medium was not due to an inefficiency of the cell model and was not dependent on the specific features of its own signal peptide. Furthermore, immunofluorescence analysis on transfected cells showed that the intracellular Emilin-3 co-localized with D1ER, a protein used as an endoplasmatic reticulum marker, indicating that the transfected protein was properly delivered to the cell secretory pathway (Fig. 7C). Interestingly, some Emilin-3 was also found to be deposited onto the coverslip, suggesting that the protein can be secreted by transfected cells and that it can be detected in an extracellular context (Fig. 7C).

Emilin-3 is associated with the extracellular matrix via heparin or heparan sulfate proteoglycans

The lack of noticeable levels of Emilin-3 in the conditioned media of transfected cells suggested the hypothesis that the protein might become bound to components of the extracellular matrix (ECM). Accordingly, the insoluble material that remained associated with the culture dish was examined. Cell lysates were prepared by lysing cells in the culture dish using RIPA buffer at 4°C. After removal of cell lysate, culture dishes were washed three times with RIPA buffer and material that remained bound to the dish was extracted with Laemmli buffer at 90°C. As shown in Fig. 8, this ECM fraction was found to contain a relatively high amount of Emilin-3 protein. Interestingly, this ECM-associated Emilin-3 migrated slightly slower than the protein associated within the cell layer, suggesting that some post-translational modifications occurred just before the secretion of the protein (Fig. 8). A number of secreted proteins and growth factors are thought to associate with the ECM becuse of their affinity for heparin and heparan sulfate proteoglycans (Bernfield et al., 1999). Therefore, the possibility that Emilin-3 may also have heparin-binding properties was investigated. Towards this aim, soluble heparin was added to the culture medium of transfected HEK293T cells. Whereas little or no Emilin-3 was present in the conditioned medium of cells grown under normal conditions, the protein could be easily detected in the medium when transfected cells were grown in the presence of 50 μg/ml of soluble heparin. Furthermore, heparin addiction reduced the amount of the protein associated to the ECM and desposited on the coverslip as shown by immunoflurescence on transfected cells (Fig. 8B). Although there are several possible interpretations for

this observation, the data raises the possibility that soluble heparin in the medium may compete with the ECM binding of Emilin-3.

Emilin-3 binds heparin through its EMI domain

In order to test directly the possibility that Emilin-3 may bind heparin, lysates of transfected cells were incubated with heparin-agarose beads. The material bound to the beads was then eluted with a series of buffers with different salt concentrations and analyzed by western blot. As shown in Fig. 9, Emilin-3L was efficiently bound to the heparin-agarose beads and eluted with washes between 0.4 and 1.2 M NaCl. This association was specifically dependent on the heparin moiety since the Emilin-3L protein did not bind to unconjugated agarose beads. With a similar setup, the same results were also obtained for Emilin-3S. (Fig. 9A) To determine which fragment of Emilin-3 is required for heparin binding, an Emilin-3 construct lacking the cysteine-rich EMI domain (Emilin-3ΔEMI) was generated. Interestingly, the Emilin-3ΔEMI recombinant protein did not bind to heparin-conjugated beads, suggesting that the EMI domain is necessary for the association to heparin. Accordingly, the Emilin-3ΔEMI protein could be easily detected in the conditioned medium of transfected cells (Fig. 9B). Therefore, the EMI domain mediates, at least in part, the association of Emilin-3 with the ECM.

The gC1q domain is dispensable for Emilin self-assembly

It has been proposed that the C-terminal C1q domain of Emilin-1 might play an important role in Emilin-1 multimeric assembly (Mongiat, et al. 2000). Since Emilin-3 is able to form disulfide-bonded trimers (see also Fig. 7), although it lacks the gC1q domain, I investigated whether the cysteine-rich EMI domain has a role in trimer and/or multimer formation of Emilins. Towards this aim, recombinant Emilin-1 constructs lacking either the gC1q domain or the EMI domain were produced and transfected into HEK293T cells together with Emilin-3 constructs. Under non-reducing condtions, all these recombinant proteins were able to form homotrimers, indicating that neither the gC1q nor the EMI domain are indispensable for this process (Fig. 10A). Furthermore, formation of higher order multimers was studied by electrophoresis with agarose-acrylamide composite gels under non-reducing conditions. Emilin-1, Emilin-1ΔgC1q and Emilin-3 were found almost exclusively in large aggregates reaching 2000 kDa. By contrast, Emilin-1ΔEMI and Emilin-3ΔEMI aggregated with a lower efficiency. In particular, almost no high molecular weight multimers of Emilin-1ΔEMI were detected in these experiments (Fig. 10B). Collectively, these data demonstrate that the gC1q domain is not necessary for trimer and multimer formation and suggest a role for the EMI domain in the formation of higher order multimers.

Emilin-3 undergoes N-glycosylation

Since the sequence of Emilin-3 contain four predicted N-glycosylation sites, has been investigated whether the observed molecular weight shift between the protein associated with the cell layer and the secreted protein could be the consequence of glycosylation. Concentrated conditioned medium and cell lysate of Emilin-3 transfected cells were treated with different enzymes to remove either N-linked or O-linked carbohydrates, and the treated samples were analyzed by western blot. This experiment clearly showed that Emilin-3 post-traslational modifications are entirely due to N-glycosylation, since the treatment with the PNGase F endoglycosidase was sufficient to convert Emilin-3 to its non-processed molecular weight (Fig. 11).

Emilin-3 distribution in embryonic and adult tissues

Immunoprecipitation experiments using two different Emilin-3 specific antibodies (rabbit and guinea pig) demonstered that both Emilin-3L and Emilin-3S are effectively produced *in vivo* and that these proteins could form homotrimers as observed with *in vitro* experiments (Fig. 12A). Furthermore, immunohistochemical analysis revealed that the Emilin-3 protein has a wider distribution compared with the mRNA expression. Emilin-3 is indeed found in the connective tissues of several tissues with a clear extracellular pattern. As observed for mRNA species , the protein is particularly abundant during embryonic life. At E14.5 Emilin-3 is found throughout the embryo in mesenchymal tissues. Pericondrium of developing long bones, vibrissae, developing gonads, subepidermal mesenchyme, developing muscle and myoenteric plexus of the gastrointestinal tract are among the more labeled structures. In adult mice the distribution of the protein is much more restricted. Emilin-3 has been detected in the basament membrane of the seminiferous tubules, in some skeletal muscle, surrounding the myoenteric plexus of all the gastroinestinal tract, around hair follicls, in the uterus and in different cartilaginous structures (Fig. 12B).

Emilin-3 interacts with Emilin-1

Immunohistochemical analysis in embryonic tissues showed that Emilin-1 and Emilin-3 distribution overlaps almost completely. In particular, while Emilin-1 seems to have a more diffuse deposition, all the Emilin-3 staining overlaps with Emilin-1. Double immunostaining of transverasl sections of E14.5 mouse forelimb are shown in figure 13A. Emilin-3 antibody strongly stained the perichondrium of developing metacarpal bones, while no staining was detected in the carilaginous core. On the other hand, at the same level, Emilin-1 is present both in perichondria and in cartilages. Interestingly where the two proteins are both expressed, they

overlap completely. As previoulsy revealed by our in situ hybridization studies, both proteins are expressed in the gastrointestinal tract even with a different pattern. Again, immunofluorescence experiments in the developing gut showed a partial overlap between Emilin-1 and Emilin-3 deposition (Fig13B): while Emilin-1 is distributed throughout the wall of the embryonic midgut, Emilin-3 is present in a thinner layer around the myoenteric neurons overlapping with Emilin-1. These observations suggest the possibility of a physical interaction between the two proteins. To directly test this hypotesis, co-immunoprecipitation experiments on transfected HEK293T cells have been carried out using different Emilin-1 and -3 constructs (Fig. 13C). Both Emilin-3 and Emilin-3ΔEMI could be immunoprecipitated by Emilin-1 and Emilin-1ΔgC1q (not shown) indicating that this interaction is not dependent from EMI nor gC1q domains. Non reduced gels showed no clear shifts in the migration pattern of immunoprecipitated protein trimers, suggesting that the two proteins are not forming heterotrimeric aggregates.

Zebrafish Emilin-3 paralogs are localized in the basement membrane of the notochord

It has been previously shown that both *emilin3a* and *-3b* genes are strongly expressed in the zebrafish notochord at early developmental stages (Milanetto, et al. 2008). To investigate the protein distribution during zebrafish development, whole mount immunofluorescence experiments were performed with a polyclonal rabbit antiserum raised against the recombinant Emilin-3 murine protein. At the 20-somite stage, a strong signal was detected in the notochord, particularly in the posterior region of the embryo (Fig. 14A). The signal colocalized in part with collagen II, one of the most abundant component of the peri-notochordal basement membrane. At 24 hpf, Emilin-3 signal was detected as a continuous thin layer lining the notochord with a posterior-anterior gradient that resembled *Emilin3* mRNAs expression pattern (Fig. 14B). Interestingly, in agreement with *Emilin3* mRNAs expression in the notochord, which is turned off soon after 24 hpf, no Emilin-3 protein signal could be detected anymore around the notochord at 48 hpf (not shown), suggesting that Emilin-3 protein could have a rapid turnover in the ECM. The notochord is normally surrounded by a three layered ECM sheath that is commonly called the peri-notochordal basement membrane (Stemple, 2005). To assess whether Emilin-3 was present in this structure, double immunostaining for Emilin-3 and collagen II was performed. While collagen II was found also into the notochord bulk, Emilin-3 colocalized with the fraction of collagen II located in the notochord sheath, demonstrating for the first time that Emilin-3 is a component of the peri-notochordal basement membrane (Fig. 14C).

Emilin3a and -3b are essential for notochord development

To investigate the functional role of the two zebrafish Emilin-3 paralogs during early embryonic development, fish embryos at one- or two-cell stages were subjected to targeted knock-down by microinjection of morpholino oligonucleotides designed to block the splicing process between the first exons and introns of *emilin3a* and *emilin3b*. In these experiments, a universal control morpholino oligonucleotide was also injected, to ensure that the observed phenotypes were not caused by the injection procedure. Embryos injected with morpholinos for *emilin3a* and *emilin3b* developed normally until 24 hpf stage, when they started to look shorter then control embryos, ventrally curved and displaying a striking distortion of the normal notochord rod-like appearance (Fig. 15A). The effect of the injected morpholinos was confirmed by RT-PCR experiments, showing that *emilin3a* and *-3b* mRNA were almost completely absent in morphant embryos perhaps due to RNA degradation processes caused by intron retention. Furthermore, immunofluorescence experiments with Emilin-3 antiserum showed that the specific labeling of the notochord sheath was totally missing from the morphant embryos at 24 hpf. The phenotypic effects of the double morphant embryos were dependent from the injected morpholinos concentrations (Fig. 15B). Morphant embryos were observed until day 7 after fertilization, but no other macroscopic defects were observed except for those described above. Interestingly, the most evident defect observed in *emilin3a* and *-3b* morphants was a marked descrease of motility.

To confirm that the observed phenotypes were the consequence of *emilin3a* and *-3b* inactivation, a second knockdown strategy was used. For this purpose, one-or two-cell stage zebrafish embryos were microinjected with two morpholino oligonucleotides designed to recognize the *emilin3a* and *-3b* translation initiation codons in order to block their translation. Noteworthy, at 24 hpf, injected embryos displayed the same phenotypes observed with the splicing blocking morpholinos and the effects were again dose-dependent (Fig. 16). A further confirmation of the specificity of this phenotype was obtained by injection experiments with mixed morpholinos (i.e. injection of a splicing morpholino directed against one paralogue togheter with a translational blocking morpholino for the other paralogue), which recapitulated the expected phenotype. Altogether, these data demonstrate that Emilin-3 has an essential role in notochord development.

Zebrafish *emilin3a* and *-3b* genes have an overlapping and markedly similar expression pattern, as both genes are expressed in the notochord with a similar time course (Milanetto, et al. 2008). Thus, it can be easily speculated that they may also have a redundant function during notochord development. To directly test this hypothesis, morpholino oligonucleotides against *emilin3a* and *emilin3b* were injected singularly in zebrafish embryos (Fig. 18). Interestingly, injection of a single morpholino did not cause any overt phenotype even at very high concentration (not shown), suggesting that the two Emilin-3 paralogs have a similar role in the mantainance of the normal structure of the developing notochord.

Electron microscopy reveals notochord abnormalities in Emilin3 double morphant embryos

Since the notochordal sheath is a strong and flexible structure with an important mechanical role, needed for mantaining the normal notochord shape and opposing resistence to the pressure generated by vaculating notochordal cells, it is reasonable to hypothesize that defects in the notochord basement membrane may cause the phenotype observed in *emilin3a* and *-3b* double morphant embryos. To directly test this possibility, transversal sections at the trunk level of 30 hpf embryos injected with control or *emilin3a/3b* morpholino oligonucleotides were investigated by transmission electron microscopy. While the three layer of the peri-notochordal basement membrane looked normal in embryos injected with control morpholino, the middle layer displayed alterations in the *emilin3a/3b* morphant embryos: in particular, the longitudinal collagen fibers looked weavy and frequently interrupted and the entire middle layer appeared thicker (Fig. 19). This observation implies that extracellular deposition of Emilin-3 in the basement membrane of the notochord is necessary for the normal organization of this structure.

Aberrant col2a1 expression by nothocordal cells of emilin3a/3b double morphant embryos

To further characterize the phenotype of *emilin3a/3b* double morphant embryos, whole mount in situ hybridization experiments were carried out for some of the most important notochordal marker genes in 24 hpf morphant and control embryos. No differences were found for *no tail* and *sonic hedgehog* genes, while *col2a1* transcript was clearly upregulated in morphant embryos ad 24 hpf and 30 hpf (Fig. 20 and data not shown). *col2a1* is normally expressed by notochordal cells before vacuolation and it completely disappears in the nothocord by 24 hpf, when the expression is mantained in hypochordal and floorplate cells until 48 hpf (Yan et al., 1995). Interestingly, *col2a1* expression was mantained in the notochordal cells of *emilin3a/3b* double morphant embryos also at 48 hpf (Fig. 20), suggesting that the signal that normally turns off *col2a1* expression is missing in Emilin-3 deficient notochords. Furthermore, whole-mount immunofluorescence experiments showed that collagen II is upregulated in Emilin-3 deficient embryos not only at the mRNA level, but also at the protein level (Fig. 21A). At 48 hpf, some *emilin3a/3b* morphant embryos showed also an ectopic *col2a1* expression in the intersomitic spaces and in the caudal reticular venous plexus, and collagen II protein was detected in some cells localized far away from the notochord (Fig. 21B). This observation suggests that the deficiency of Emilin-3 from the notochordal basement membrane causes a dysregulation of some signal, inducing collagen II ectopic expression. At the moment, the nature of this signal remains unknown. It is important to remember here that *col2a1* upregulation was previously detected in other embryos with notochord defects, such as collagen VIII

and fibrillin-2 mutants (Gansner et al., 2008a and 2008b) and embryos with inhibition of the activity of lysyl oxidases (Gansner et al., 2007).

The notochord of emilin3a/3b morphant embryos is sensitized to lysyl oxidase inhibition

Lysyl oxidases are copper-dependent enzymes that stabilize ECM by crosslinking elastin and collagens (Csiszar, 2001; Kagan and Li, 2003), a process thought to be important for the maintainance of notochord sheath integrity during notochord vacuolation. The human genome contain five genes encoding for lysyl oxidase family members, characterized by the presence of a conserved copper binding domain and residues for a lysyl-tyrosyl quinone cofactor. Although experimental evidence suggests a role for two of these lysyl oxidases in elastin and collagen crosslinking (Hornstra et al., 2003; Liu et al., 2004; Maki et al., 2002; Maki et al., 2005), the precise role of each family member in ECM formation, cancer biology, and intracellular signaling remains poorly understood. Recently, eight unique zebrafish lysyl oxidase genes were cloned, suggesting that some of the human genes are duplicated in *Danio rerio* (Gansner et al., 2007; Lynch and Force, 2000; Woods et al., 2000). The chemical compound β-aminopropionitrile (βAPN) irreversibly inhibits lysyl oxidases by binding the active site of the catalytic domain (Molnar et al., 2003; Tang et al., 1983). Interestingly, incubation of 3 hpf zebrafish embryos with 10 mM βAPN resulted in a striking notochord distortion that was highly similar to the phenotype observed in *emilin3a/3b* double morphant embryos (Fig. 22). While βAPN acts on all lysyl oxidase isoforms, morpholino experiments showed that knockdown of *loxl1* or *loxl5b* genes is sufficient to cause the notochordal phenotype (Gansner et al., 2007). To investigate whether Emilin-3 may have some functional interaction with lysyl oxidases, zebrafish embryos were injected with low doses of Emilin-3 morpholinos alone or in combination with a sub-toxic concentration of βAPN (1 mM). Strikingly, only the embryos that received the two combined treatments displayed the expected phenotype, suggesting the possibilty of a functional interaction between Emilin-3 and lysyl oxidase activity in the maintenance of the notochord sheath structure.

Muscle abnormalities in Emilin-3 double morphant embryos

Beyond its essential structural role, the notochord has several well-established roles in patterning the surrounding tissues (Clever and Krieg, 2001; Dodd et al., 1998; Hogan and Bautch, 2004; Holland et al., 2004; Stemple, 2005). Among others, notochord plays a role in muscle specification and development. In particular, in teleosts, notochord-derived Hedgehog signals control the formation of the horizontal myoseptum, as well as specifying muscle cell fates (Barresi et al.,

2000; Devoto et al., 1996; Wolff et al., 2003). Semithin sections at the trunk level of Emilin-3 double morphant embryos at 30 hpf revealed some alteration in somite organization. Myotomes were larger and disorganized compared to control embryos and some cells in the medial part of the somites, just in close proximity of the notochord sheath, were abnormally vacuolated (Fig. 23A). To further characterize these findings, embryos injected with *emilin3a/3b* and control morpholinos were stained with phalloidin-FITC to visualize actin and assess the overall muscle morphology. Except for a slight disorganization of muscle fibers, myotomes shape and muscle fibers appeared normal in Emilin-3 morphant embryos (Fig. 23B). In agreement with this, staining for the fast myosin heavy chain-1 that marks fast muscle fibers detected no obvious anomalies in Emilin-3 morphant embryos, as expected (Fig. 23C). Indeed, fast fibers originate from the lateral plate mesoderm, which is not in direct contact with the notochord basement mebrane. On the other side, different types of slow muscle fibers (slow muscle cells, muscle pioneers and medial fast fibers) develop from a common cell population, the adaxial cells, that are in close contact with the basement membrane of the notochord (Ochi and Westerfield, 2007). Engrailed is a known marker of these cells, where high Engrailed expression marks muscle pioneers while low Engrailed expression characterizes fast medial fibers (Ochi and Westerfield, 2007). To investigate whether knockdown of Emilin-3 affects the normal differentiation of these cell types, morphant embryos were stained for the Engrailed protein. Interestingly, Emilin-3 double morphant embryos displayed a partial alteration of muscle specification. Indeed, although morphant embryos displayed an overall normal staining for the fast myosin heavy chain, both high and low Engrailed positive cells were significantly increased (Fig. 24). Since both muscle pioneers and fast medial fibers are positively regulated by the Hedgehog signaling (Wolff et al., 2003) and negatively by BMP signaling (Dolez et al., 2011), Emilin-3 deficency could cause either an increased Hedgehog or an impaired BMP signaling.

DISCUSSION

The Emilin/Multimerin family of secreted glycoproteins was identified few years ago (Braghetta et al., 2004). These proteins have a unique structure and domain organization among extracellular proteins, with a peculiar seven-cysteine EMI domain located at the N-terminus and a long central region with coiled-coil motifs preceding a gC1q domain at the C-terminus. With the aim of unveiling the function of Emilin proteins in vivo, our laboratory generated knockout mice for the different Emilin/Multimerin genes. All generated mice are viable and fertile, and they do not display any overwhelming phenotype. Among them, Emilin-1 null mice were the best characterized until now (Zanetti et al., 2004; Zacchigna et al., 2006). Morphological examination by light and electron microscopy revealed interruptions and irregularity of elastic lamellae of aorta and skin. These data and the finding that the protein binds to other components of elastic fibers, such as Elastin and Fibulin-5, suggested a function of Emilin-1 in elastogenesis (Zanetti et al., 2004). Moreover, analysis of the cardiovascular system revealed that Emilin-1 deficient mice are affected by systemic arterial hypertension caused by an increased peripheral resistance. This phenotype was linked to an increased TGF-β1 signalling, and it was demonstrated that Emilin-1 prevents TGF-β1 maturation thus reducing the availability of active TGF-β1 (Zacchigna et al., 2006). These findings rise the captivating idea that Emilin proteins may play a role in the regulation of growth factor activity in the extracellular enviroment.

It is well estabilished that ECM structural macromolecules operate as platforms to which growth factors of the TGF-β superfamily are targeted and concentrated (ten Dijke, 2007). Pro-domains of these growth factors are the molecular mediators of interactions with several ECM proteins, and in particular TGF-β family members are known to be secreted in the form of a covalent complex with LTBP proteins (Rifkin, 2005). LTBP proteins, in turn, bind different ECM components, thereby incorporating the different TGF-β isoforms into ECM in a latent form. The TGF-β/LTBP interaction is mediated by disulfide bonds between Cys-33 of the TGF-β pro-domain (LAP) with specific cysteines in the TB modules of LTBP proteins (Saharinen et al.,1996). Noteworthy, the LAP pro-domain contains only other two cysteines residues that are necessary for the homodimerization of the molecule (Brunner et al., 1989). It was demonstrated that Emilin-1 is able to bind pro-TGF-β1 preventing its processing to the mature form in the extracellular enviroment, but the precise molecular mechanisms of this interaction were not fully elucidated. The results presented in this thesis show for the first time the intriguing possibility that Emilin-1 binds the pro-TGF-β molecule with a disulfide bridge between Cys-33 of LAP and yet unidentified cysteine residues in Emilin-1 protein. Furthermore, it was demonstered here that the interaction of Emilin-1 with pro-TGF-β1 occurs independently from the cysteine-rich EMI domain but further experiments will be required to define the cysteines of Emilin-1 that are binding LAP-β1.

This findings contribute to expand the general concept of growth factor targeting in the ECM, suggesting in particular that TGF-β family members could have more than one partner (other than LTBP proteins or fibrillins) for the targeting in different contexts of the ECM. Thus, TGF-β factors could be secreted in inactive

forms in at least two different pools (bound to either LTBPs or Emilin-1, since they seem to share the same cysteine of LAP), in association with different proteins and activated by different mechanisms for the fine tunings of their activity in different tissues and conditions. Further studies will be necessary to define more precisely the molecular mechanisms of this interaction and understand its biological significance.

However, the main focus of this thesis was another member of the Emilin/Multimerin family: Emilin-3. Emilin-3 lacks the C-terminal gC1q domain conserved in all other Emilins/Multimerins, thus the structural organization of Emilin-3 makes it a peculiar member of the family. Expression studies during mouse embryogenesis revealed another unique feature, as *Emilin3* gene is not expressed in the cardiovascular system where all Emilins/Multimerins are abundantly present. As previously shown for all the other Emilin genes, expression of *Emilin3* decrease drastically in the adult life, when few tissues (i.e. eye and testis) are still positive for its transcripts. Furthermore, *Emilin3* is the only Emilin gene for which alternatively spliced isoforms were detected. At least in mouse, two *Emilin3* transcripts are present: a full length transcript (*Emilin3L*) and a transcript lacking the first 141 bp of the fourth exon (*Emilin3S*). No *Emilin3* splicing variants were found in human cell lines (data not shown), suggesting that this process may not be a general feature in mammals. Interestingly, one of the two zebrafish Emilin-3 paralogs, *emilin3b,* also seems to undergo alternative splicing (data not shown).

In situ hybridization experiments showed that *Emilin3* has a dynamic expression pattern during mouse development. At the E8.5 stage, expression is detected in in the tail bud region, a structure known to contain a multipotent stem cell population. At E9.5, Emilin3 expression is also detectable in the primitive gut, and expression in the gastro-intestinal system persists throughout the development until adult life. Further studies will be required to understand whether *Emilin3* is expressed either by neuronal cells or by the supporting cells. Strong expression during mouse development was detected in the genital ridge, in some skeletal muscles, such as diaphragm, and in the mesenchymal condensations giving rise to cartilage and bones. Emilin-3 protein distribution was also investigated by immunofluorescence. Deposition of Emilin-3 protein in the extracellular space during mouse development overlaps with the mRNA expression pattern but is somewhat more diffuse. The protein indeed seems to accumulate in the ECM, also in tissues where the transcript cannot be detected. In adult tissues, Emilin-3 protein distribution is quite restricted. Emilin-3 is abundant in the basement membrane of seminiferous tubules of testis of adult mice. A strong Emilin-3 labeling was also observed throughout the gastro-intestinal tract in close association with the myoenteric plexus, with the strongest signal in the esophagus. Emilin-3 is also present in adult skeletal muscles, with a peculiar distribution around few muscle fibers. Collectively, these data represent the first detailed description of the expression and protein distribution of Emilin-3 in mouse.

Further studies using a transIent transfection system in HEK293T cells provided some interesting information about Emilin-3 biochemical properties. Emilin-3 displayed an higher affinity for the ECM of cultured cells than other Emilins.

Indeed, while Emilin-1 and Emilin-2 are efficently secreted in the conditioned medium of transfected cells, almost all the secreted Emilin-3 is found associated to the ECM. Interestingly, the addition of soluble heparin to the culture medium significantly enhanced the presence of Emilin-3 in the medium, indicating the possibility the Emilin-3 may associate with the ECM via heparin or other heparan-sulphate proteoglycans. The observation that Emilin-3 binds heparin confirmed this hypothesis. The finding that Emilin-3 is an heparin-binding protein is of particular interest, considering that heparan-sulphate proteoglycans have been shown to interact with various ligands involved in the regulation of embryonic development, including Wnt family members (Bernfield et al., 1999), FGFs (Yayon et al., 1991) TGF-βs, BMPs (Yamaguchi et al., 1990; Jackson et al., 1997) and Sonic Hedgehog (Rubin et al., 2002). Thus, it is possible that Emilin-3 binding to heparan-sulfate proteoglycans in the ECM *in vivo* may also influence the availability of some of these "heparin-binding" growth factors. Furthermore, it will be interesting to explore if other Emilins possess this property, since the heparin-binding activity of Emilin-3 seems to be located in the EMI domain that is highly conserved among all proteins of the Emilin/Multimerin family.

Another information obtained by transfection studies is that the gC1q is dispensable for multimerization of Emilins. Indeed, although it has been shown that the Emilin-1 gC1q domain can form homotrimers in analogy with several other members of the TNF/C1q superfamily of proteins (Mongiat et al., 2000), the experiments reported here clearly demonstrate that Emilin-3, which naturally lacks the gC1q domain, as well as a recombinant Emilin-1 protein lacking the gC1q domain, are both able to form homotrimers via intermolecular disulfide bonds. On the other hand, the same experiments revealed for the first time a role for the EMI domain in the assembly of higher order multimers of Emilins. Furthermore, these experiments indicated for the first time the interaction between two different Emilin members both in vitro and in vivo. Although the hypotesis of an interaction between different Emilin members was already formulated before (Doliana et al., 2000 and 2001), no definitive proof was produced to date. Here it is reported that, at least during mouse development, Emilin-1 and Emilin-3 deposition is partially overlapping indicating that the two protein could indeed interact *in vivo*. Furthermore, *in vitro* experiments demonstrated that Emilin-1 and Emilin-3 can interact in a process that is independent from both the EMI and the gC1q domains. The possibility that the two proteins could form covalently bound heterotrimeric aggregates will need more experiments to be confirmed or ruled out.

To investigate the function of Emilin-3 *in vivo*, the zebrafish model was exploited. Eight Emilin/Multimerin paralogs were previously identified in the zebrafish genome, corrisponding to four mammalian Emilin/Multimerin genes (Milanetto et al., 2008). Among them, the two Emilin-3 paralogs, *emilin3a* and *emilin3b*, showed the most peculiar expression pattern. They are both expressed in a very similar manner in the notochord of zebrafish embryos until 24 hpf, while at later stages both Emilin-3 transcripts are found in the mesenchyme and cartilage primordia of craniofacial developing skeleton (Milanetto et al., 2008). Interestingly, this expression pattern is fully in agreement with that of their murine ortholog. To investigate the function of Emilin-3 in zebrafish development, the morpholino-based knockdown strategy was employed, with the injection of different

morpholinos targeting either the splicing sites of first exon and intron or the ATG start codon of zebrafish *emilin3a* and *emilin3b*. Loss of both Emilin-3 transcripts led to defects in the peri-notochordal basement membrane and notochord structures, and *emilin3a/-3b* morphant embryos displayed anatomical alterations with a shorter size and wavy notochord shape.

The peri-notochordal basement membrane is composed of a variety of ECM molecules that interact to facilitate the anchorage of notochordal cells, and loss of one of these components disrupts the basement membrane organization. Laminin-1 and collagen IV are the major components of mammalian basement membranes, including the peri-notochordal basement membrane. Removal of laminin α1, β1 and γ1 chains prevents formation of the basement membrane surrounding the notochord (Pollard et al., 2006; Parsons et al., 2002). Knockdown of laminin β1, γ1 and α1 (Paulus and Halloran, 2006) phenocopies grumpy (gup), sleepy (sly) and bashful (bal) mutants respectively, which all present a disrupted peri-notochordal basement membrane. The peri-notochordal sheath is composed of three different ECM layers, two of which are composed of dense bundles of collagen fibrils. Interestongly, Emilin-3 knockdown leads to the disruption of the peri-notochordal sheath, as demonstrated by electron microscopy that showed disorganized fibrils in the middle layer. Moreover, the structural alterations in peri-notochordal basement membrane of Emilin-3 knockdown fish result in defects of notochord differentiation, such as the abnormal persistence of *col2a1* expression as demonstrated by *in situ* hybridization and Collagen II immunofluorescence. In agreement with the overlapping expression of both Emilin-3 paralogs, single knockdown of either *emilin3a* or *emilin3b* does not recapitulate the phenotype of the double morphant embryos, indicating that the two paralogue genes play a redundant role in the notochord development. It was recently reported that lysyl oxidase activity is required for the normal formation of the zebrafish notochord and that lysyl oxidase inhibition both via pharmacological inhibition or morpholino mediated knockdown causes a notocord phenotype (Gansner et al., 2007). As also experimentally confirmed here, the phenotype of zebrafish embryos with pharmacological inhibition lysyl oxidase activity is remarkably similar to the one observed in Emilin-3 morphant embryos. Double treatment experiments indicated a functional interaction between Emilin-3 and lysyl oxidase activity in maintaining the correct structure of the notochord. This finding suggest the possibility that Emilin-3 could be a target or a regulatory component of the lysyl oxidase activity or that they maintain the normal structure of the notochordal sheath by completely different mechanisms.

During embryonic development, Emilin-3 is expressed later than laminin α1, β1 and γ1 chains, which exhibit a maternal expression whereas *emilin3a* and *-3b* transcripts are first detected at 10 hpf (Milanetto et al., 2008). Thus, Emilin-3 cannot be involved in the early differentiation of notochord. However, it cannot be ruled out that Emilin-3, like laminins, may act directly on notochord differentiation. The most likely hypothesis is that loss of Emilin-3 perturbs either the cell attachment to the basement membrane or the deposition and activation of secreted growth factors associated with the basement membrane, leading to a dysregulation of associated signals. Although these findings indicate that Emilin-3 knockdown alters the ECM architecture of the developing notochord, it is not yet

known whether this alteration is directly caused by Emilin-3 deficency or it is a seconday effect, for instance, of an increased vacuolation process of the notochordal cells. Furthermore, it is not clear yet whether the alteration of the notochordal basement membrane is a developmental defects or a degenerative effect. Further studies will be required to answer to these questions.

To explore the idea that Emilin-3 deficiency may be associated with signaling defects, muscle development was investigated in Emilin-3 double morphant embryos. In fact, it is well estabilished that notochord-derived Hedgehog signals are sufficient for the specification of different muscle cell types (Wolff et al., 2003). In particular, these notochord-derived signals are important for the specification of adaxial cells in slow muscle, fast medial fibers and muscle pioneers, three subtypes of myofibers with different morphologies and molecular markers (Hirsinger et al., 2004; Ochi and Westerfield, 2007). Since Emilin-3 is expressed by notochord cells with a spatio-temporal pattern similar to that of Hedgehog ligands Sonic Hedgehog or Echidna Hedgehog (Currie and Ingham, 1996), differentiation of slow muscle cells was analyzed in Emilin-3 morphants. Strikingly, while no differencies were observed in the developing fast fibers (that derive from the lateral plate mesoderm with a different mechanism), both medial fast fibers and muscle pioneers number was increased in emilin3a/-3b double morphant embryos, as demonstrated by staining for the Engrailed transcription factor. Since Engrailed expression is positively regulated by Hedgehog (Wolff et al., 2003) and negatively by BMP signaling (Dolez et al., 2011), both pathways could be affected in Emilin-3 deficient embryos. Interestingly, Hedgehog and BMP ligands can be both regulated by heparan sulfate proteoglycans (Eugster et al., 2007; Rider,2006) and a role for heparan sulfate proteoglycans in zebrafish myofiber differentiation has been recently proposed (Dolez et al., 2011). Further in vitro and in vivo experiments will help elucidating the role of Emilin-3 in the control of extracellular growth factors other than TGF-βs.

In summary, the data reported in this thesis provide the first detailed characterization, with both structural and functional insights, of the extracellular glycoprotein Emilin-3. The findings of this study will be the basis for further *in vitro* and *in vivo* studies in mouse and zebrafish, with the aim of fully understanding the biological role of this peculiar member of the Emilin/Multimerin family in embryonic development and in tissue homeostasis.

REFERENCES

Adams, D., Keller, R., & Koehl, M. (1990). The mechanics of notochord elongation, straightening and stiffening in the embryo of Xenopus laevis. *Development (Cambridge, England) , 110* (1), 115-30.

Adams, J., & Watt, F. (1993). Regulation of development and differentiation by the extracellular matrix. *Development (Cambridge, England) , 117* (4), 1183-98.

Amacher, S., & Kimmel, C. (1998). Promoting notochord fate and repressing muscle development in zebrafish axial mesoderm. *Development (Cambridge, England) , 125* (8), 1397-406.

Amma, L., Goodyear, R., Faris, J., Jones, I., Ng, L., Richardson, G., et al. (2003). An emilin family extracellular matrix protein identified in the cochlear basilar membrane. *Molecular and cellular neurosciences , 23* (3), 460-72.

Angel, P., Nusinow, D., Brown, C., Violette, K., Barnett, J., Zang, B., et al. (2010, Dec 6). Networked-based Characterization of Extracellular Matrix Proteins from Adult Mouse Pulmonary and Aortic Valves. *Journal of Proteome Research* , 101206131312002.

Arteaga-Solis, E., Gayraud, B., Lee, S., Shum, L., Sakai, L., & Ramirez, F. (2001). Regulation of limb patterning by extracellular microfibrils. *The Journal of cell biology , 154* (2), 275-81.

Aszódi, A., Chan, D., Hunziker, E., Bateman, J., & Fässler, R. (1998). Collagen II is essential for the removal of the notochord and the formation of intervertebral discs. *The Journal of cell biology , 143* (5), 1399-412.

Bernfield, M., Götte, M., Park, P., Reizes, O., Fitzgerald, M., Lincecum, J., et al. (1999). Functions of cell surface heparan sulfate proteoglycans. *Annual review of biochemistry , 68*, 729-77.

Berrier, A., & Yamada, K. (2007). Cell-matrix adhesion. *Journal of cellular physiology , 213* (3), 565-73.

Bertrand, J., Chi, N., Santoso, B., Teng, S., Stainier, D., & Traver, D. (2010). Haematopoietic stem cells derive directly from aortic endothelium during development. *Nature , 464* (7285), 108-11.

Bressan, G., Castellani, I., Colombatti, A., & Volpin, D. (1983). Isolation and characterization of a 115,000-dalton matrix-associated glycoprotein from chick aorta. *The Journal of biological chemistry , 258* (21), 13262-7.

Bressan, G., Daga-Gordini, D., Colombatti, A., Castellani, I., Marigo, V., & Volpin, D. (1993). Emilin, a component of elastic fibers preferentially located at the elastin-microfibrils interface. *The Journal of cell biology , 121* (1), 201-12.

Charbonneau, N., Ono, R., Corson, G., Keene, D., & Sakai, L. (2004). Fine tuning of growth factor signals depends on fibrillin microfibril networks. *Birth defects research Part C, Embryo today : reviews , 72* (1), 37-50.

Chaudhry, S., Cain, S., Morgan, A., Dallas, S., Shuttleworth, C., & Kielty, C. (2007). Fibrillin-1 regulates the bioavailability of TGFbeta1. *The Journal of cell biology , 176* (3), 355-67.

Christ, B., Huang, R., & Scaal, M. (2004). Formation and differentiation of the avian sclerotome. *Anatomy and embryology , 208* (5), 333-50.

Christian, S., Ahorn, H., Novatchkova, M., Garin-Chesa, P., Park, J., Weber, G., et al. (2001). Molecular cloning and characterization of EndoGlyx-1, an EMILIN-like multisubunit glycoprotein of vascular endothelium. *The Journal of biological chemistry , 276* (51), 48588-95.

Cleaver, O., & Krieg, P. (2001). Notochord patterning of the endoderm. *Developmental biology , 234* (1), 1-12.

Colombatti, A., Bonaldo, P., Volpin, D., & Bressan, G. (1988). The elastin associated glycoprotein gp115. Synthesis and secretion by chick cells in culture. *The Journal of biological chemistry , 263* (33), 17534-40.

Colombatti, A., Bressan, G., Castellani, I., & Volpin, D. (1985). Glycoprotein 115, a glycoprotein isolated from chick blood vessels, is widely distributed in connective tissue. *The Journal of cell biology , 100* (1), 18-26.

Csiszar, K. (2001). Lysyl oxidases: a novel multifunctional amine oxidase family. *Progress in nucleic acid research and molecular biology , 70*, 1-32.

Currie, P., & Ingham, P. (1996). Induction of a specific muscle cell type by a hedgehog-like protein in zebrafish. *Nature , 382* (6590), 452-5.

Dabovic, B., Chen, Y., Colarossi, C., Obata, H., Zambuto, L., Perle, M., et al. (2002). Bone abnormalities in latent TGF-[beta] binding protein (Ltbp)-3-null mice indicate a role for Ltbp-3 in modulating TGF-[beta] bioavailability. *The Journal of cell biology , 156* (2), 227-32.

Dallas, S., Park-Snyder, S., Miyazono, K., Twardzik, D., Mundy, G., & Bonewald, L. (1994). Characterization and autoregulation of latent transforming growth factor beta (TGF beta) complexes in osteoblast-like cell lines. Production of a latent complex lacking the latent TGF beta-binding protein. *The Journal of biological chemistry , 269* (9), 6815-21.

Danos, M., & Yost, H. (1995). Linkage of cardiac left-right asymmetry and dorsal-anterior development in Xenopus. *Development (Cambridge, England) , 121* (5), 1467-74.

Dietz, U., Ziegelmeier, G., Bittner, K., Bruckner, P., & Balling, R. (1999). Spatio-temporal distribution of chondromodulin-I mRNA in the chicken embryo: expression during cartilage development and formation of the heart and eye.

Developmental dynamics : an official publication of the American Association of Anatomists , 216 (3), 233-43.

Discher, D., Mooney, D., & Zandstra, P. (2009). Growth factors, matrices, and forces combine and control stem cells. *Science (New York, NY) , 324* (5935), 1673-7.

Doi, M., Nagano, A., & Nakamura, Y. (2004). Molecular cloning and characterization of a novel gene, EMILIN-5, and its possible involvement in skeletal development. *Biochemical and biophysical research communications , 313* (4), 888-93.

Dolez, M., Nicolas, J.-F., & Hirsinger, E. (2010, Nov 29). Laminins, via heparan sulfate proteoglycans, participate in zebrafish myotome morphogenesis by modulating the pattern of Bmp responsiveness. *Development (Cambridge, England)* .

Doliana, R., Bot, S., Mungiguerra, G., Canton, A., Cilli, S., & Colombatti, A. (2001). Isolation and characterization of EMILIN-2, a new component of the growing EMILINs family and a member of the EMI domain-containing superfamily. *The Journal of biological chemistry , 276* (15), 12003-11.

Doliana, R., Mongiat, M., Bucciotti, F., Giacomello, E., Deutzmann, R., Volpin, D., et al. (1999). EMILIN, a component of the elastic fiber and a new member of the C1q/tumor necrosis factor superfamily of proteins. *The Journal of biological chemistry , 274* (24), 16773-81.

Domowicz, M., Li, H., Hennig, A., Henry, J., Vertel, B., & Schwartz, N. (1995). The biochemically and immunologically distinct CSPG of notochord is a product of the aggrecan gene. *Developmental biology , 171* (2), 655-64.

Engel, J. (1989). EGF-like domains in extracellular matrix proteins: localized signals for growth and differentiation? *FEBS letters , 251* (1-2), 1-7.

Eugster, C., Panáková, D., Mahmoud, A., & Eaton, S. (2007). Lipoprotein-heparan sulfate interactions in the Hh pathway. *Developmental Cell , 13* (1), 57-71.

Fekany, K., Yamanaka, Y., Leung, T., Sirotkin, H., Topczewski, J., Gates, M., et al. (1999). The zebrafish bozozok locus encodes Dharma, a homeodomain protein essential for induction of gastrula organizer and dorsoanterior embryonic structures. *Development (Cambridge, England) , 126* (7), 1427-38.

Flaumenhaft, R., Abe, M., Sato, Y., Miyazono, K., Harpel, J., Heldin, C., et al. (1993). Role of the latent TGF-beta binding protein in the activation of latent TGF-beta by co-cultures of endothelial and smooth muscle cells. *The Journal of cell biology , 120* (4), 995-1002.

Fouquet, B., Weinstein, B., Serluca, F., & Fishman, M. (1997). Vessel patterning in the embryo of the zebrafish: guidance by notochord. *Developmental biology , 183* (1), 37-48.

Fuerer, C., Habib, S., & Nusse, R. (2010). A study on the interactions between heparan sulfate proteoglycans and Wnt proteins. *Developmental dynamics : an official publication of the American Association of Anatomists , 239* (1), 184-90.

Gansner, J., & Gitlin, J. (2008). Essential role for the alpha 1 chain of type VIII collagen in Zebrafish notochord formation. *Developmental Dynamics , 237* (12), 3715-3726.

Gansner, J., Madsen, E., Mecham, R., & Gitlin, J. (2008). Essential role for fibrillin-2 in zebrafish notochord and vascular morphogenesis. *Developmental dynamics : an official publication of the American Association of Anatomists , 237* (10), 2844-61.

Gansner, J., Mendelsohn, B., Hultman, K., Johnson, S., & Gitlin, J. (2007). Essential role of lysyl oxidases in notochord development. *Developmental biology , 307* (2), 202-13.

Garcia Abreu, J., Coffinier, C., Larraín, J., Oelgeschläger, M., & De Robertis, E. (2002). Chordin-like CR domains and the regulation of evolutionarily conserved extracellular signaling systems. *Gene , 287* (1-2), 39-47.

Geiger, B., Spatz, J., & Bershadsky, A. (2009). Environmental sensing through focal adhesions. *Nature reviews Molecular cell biology , 10* (1), 21-33.

Goldstein, A., & Fishman, M. (1998). Notochord regulates cardiac lineage in zebrafish embryos. *Developmental biology , 201* (2), 247-52.

Gregory, K., Ono, R., Charbonneau, N., Kuo, C.-L., Keene, D., Bächinger, H., et al. (2005). The prodomain of BMP-7 targets the BMP-7 complex to the extracellular matrix. *The Journal of biological chemistry , 280* (30), 27970-80.

Hayward, C., Hassell, J., Denomme, G., Rachubinski, R., Brown, C., & Kelton, J. (1995). The cDNA sequence of human endothelial cell multimerin. A unique protein with RGDS, coiled-coil, and epidermal growth factor-like domains and a carboxyl terminus similar to the globular domain of complement C1q and collagens type VIII and X. *The Journal of biological chemistry , 270* (31), 18246-51.

Hayward, C., Song, Z., Zheng, S., Fung, R., Pai, M., Massé, J., et al. (1999). Multimerin processing by cells with and without pathways for regulated protein secretion. *Blood , 94* (4), 1337-47.

Hirsinger, E., Stellabotte, F., Devoto, S., & Westerfield, M. (2004). Hedgehog signaling is required for commitment but not initial induction of slow muscle precursors. *Developmental biology , 275* (1), 143-57.

Hynes, R. (2002). Integrins: bidirectional, allosteric signaling machines. *Cell , 110* (6), 673-87.

Hynes, R. (2009). The Extracellular Matrix: Not Just Pretty Fibrils. *Science (New York, NY) , 326* (5957), 1216-1219.

Isogai, Z., Ono, R., Ushiro, S., Keene, D., Chen, Y., Mazzieri, R., et al. (2003). Latent transforming growth factor beta-binding protein 1 interacts with fibrillin and is a microfibril-associated protein. *The Journal of biological chemistry , 278* (4), 2750-7.

Iyer, A., Tran, K., Griffith, L., & Wells, A. (2008). Cell surface restriction of EGFR by a tenascin cytotactin-encoded EGF-like repeat is preferential for motility-related signaling. *Journal of cellular physiology , 214* (2), 504-12.

Jackson, S., Nakato, H., Sugiura, M., Jannuzi, A., Oakes, R., Kaluza, V., et al. (1997). dally, a Drosophila glypican, controls cellular responses to the TGF-beta-related morphogen, Dpp. *Development (Cambridge, England) , 124* (20), 4113-20.

Jasuja, R., Allen, B., Pappano, W., Rapraeger, A., & Greenspan, D. (2004). Cell-surface heparan sulfate proteoglycans potentiate chordin antagonism of bone morphogenetic protein signaling and are necessary for cellular uptake of chordin. *The Journal of biological chemistry , 279* (49), 51289-97.

Kagan, H., Sullivan, K., Olsson, T., & Cronlund, A. (1979). Purification and properties of four species of lysyl oxidase from bovine aorta. *The Biochemical journal , 177* (1), 203-14.

Lawler, J., Sunday, M., Thibert, V., Duquette, M., George, E., Rayburn, H., et al. (1998). Thrombospondin-1 is required for normal murine pulmonary homeostasis and its absence causes pneumonia. *The Journal of clinical investigation , 101* (5), 982-92.

Legate, K., Wickström, S., & Fässler, R. (2009). Genetic and cell biological analysis of integrin outside-in signaling. *Genes & Development , 23* (4), 397-418.

Leimeister, C., Steidl, C., Schumacher, N., Erhard, S., & Gessler, M. (2002). Developmental expression and biochemical characterization of Emu family members. *Developmental biology , 249* (2), 204-18.

Linsenmayer, T., Gibney, E., & Schmid, T. (1986). Segmental appearance of type X collagen in the developing avian notochord. *Developmental biology , 113* (2), 467-73.

Lohr, J., Danos, M., & Yost, H. (1997). Left-right asymmetry of a nodal-related gene is regulated by dorsoanterior midline structures during Xenopus development. *Development (Cambridge, England) , 124* (8), 1465-72.

Münsterberg, A., Kitajewski, J., Bumcrot, D., McMahon, A., & Lassar, A. (1995). Combinatorial signaling by Sonic hedgehog and Wnt family members induces myogenic bHLH gene expression in the somite. *Genes & Development , 9* (23), 2911-22.

Milanetto, M., Tiso, N., Braghetta, P., Volpin, D., Argenton, F., & Bonaldo, P. (2008). Emilin genes are duplicated and dynamically expressed during zebrafish embryonic development. *Developmental dynamics : an official publication of the American Association of Anatomists , 237* (1), 222-32.

Mohammadi, M., Olsen, S., & Goetz, R. (2005). A protein canyon in the FGF-FGF receptor dimer selects from an à la carte menu of heparan sulfate motifs. *Current opinion in structural biology , 15* (5), 506-16.

Mongiat, M., Mungiguerra, G., Bot, S., Mucignat, M., Giacomello, E., Doliana, R., et al. (2000). Self-assembly and supramolecular organization of EMILIN. *The Journal of biological chemistry , 275* (33), 25471-80.

Ng, L., Wheatley, S., Muscat, G., Conway-Campbell, J., Bowles, J., Wright, E., et al. (1997). SOX9 binds DNA, activates transcription, and coexpresses with type II collagen during chondrogenesis in the mouse. *Developmental biology , 183* (1), 108-21.

Nunes, I., Gleizes, P., Metz, C., & Rifkin, D. (1997). Latent transforming growth factor-beta binding protein domains involved in activation and transglutaminase-dependent cross-linking of latent transforming growth factor-beta. *The Journal of cell biology , 136* (5), 1151-63.

Ochi, H., & Westerfield, M. (2007). Signaling networks that regulate muscle development: lessons from zebrafish. *Development, growth & differentiation , 49* (1), 1-11.

Pagnon-Minot, A., Malbouyres, M., Haftek-Terreau, Z., Kim, H., Sasaki, T., Thisse, C., et al. (2008). Collagen XV, a novel factor in zebrafish notochord differentiation and muscle development. *Developmental biology , 316* (1), 21-35.

Parsons, M., Pollard, S., Saúde, L., Feldman, B., Coutinho, P., Hirst, E., et al. (2002). Zebrafish mutants identify an essential role for laminins in notochord formation. *Development (Cambridge, England) , 129* (13), 3137-46.

Paulus, J., & Halloran, M. (2006). Zebrafish bashful/laminin-alpha 1 mutants exhibit multiple axon guidance defects. *Developmental dynamics : an official publication of the American Association of Anatomists , 235* (1), 213-24.

Pollard, S., Parsons, M., Kamei, M., Kettleborough, R., Thomas, K., Pham, V., et al. (2006). Essential and overlapping roles for laminin alpha chains in notochord and blood vessel formation. *Developmental Biology , 289* (1), 64-76.

Pourquié, O., Coltey, M., Teillet, M., Ordahl, C., & Le Douarin, N. (1993). Control of dorsoventral patterning of somitic derivatives by notochord and floor plate. *Proceedings of the National Academy of Sciences of the United States of America , 90* (11), 5242-6.

Ramirez, F., & Dietz, H. (2009, Feb 2). Extracellular microfibrils in vertebrate development and disease processes. *The Journal of biological chemistry* .

Ramirez, F., Sakai, L., Rifkin, D., & Dietz, H. (2007). Extracellular microfibrils in development and disease. *Cellular and molecular life sciences : CMLS , 64* (18), 2437-46.

Rider, C. (2006). Heparin/heparan sulphate binding in the TGF-beta cytokine superfamily. *Biochemical Society transactions , 34* (Pt 3), 458-60.

Rifkin, D. (2005). Latent transforming growth factor-beta (TGF-beta) binding proteins: orchestrators of TGF-beta availability. *The Journal of biological chemistry , 280* (9), 7409-12.

Rubin, J., Choi, Y., & Segal, R. (2002). Cerebellar proteoglycans regulate sonic hedgehog responses during development. *Development (Cambridge, England) , 129* (9), 2223-32.

Saharinen, J., & Keski-Oja, J. (2000). Specific sequence motif of 8-Cys repeats of TGF-beta binding proteins, LTBPs, creates a hydrophobic interaction surface for binding of small latent TGF-beta. *Molecular biology of the cell , 11* (8), 2691-704.

Saharinen, J., Taipale, J., & Keski-Oja, J. (1996). Association of the small latent transforming growth factor-beta with an eight cysteine repeat of its binding protein LTBP-1. *The EMBO journal , 15* (2), 245-53.

Sakai, L., Keene, D., & Engvall, E. (1986). Fibrillin, a new 350-kD glycoprotein, is a component of extracellular microfibrils. *The Journal of cell biology , 103* (6 Pt 1), 2499-509.

Schenk, S., Hintermann, E., Bilban, M., Koshikawa, N., Hojilla, C., Khokha, R., et al. (2003). Binding to EGF receptor of a laminin-5 EGF-like fragment liberated during MMP-dependent mammary gland involution. *The Journal of cell biology , 161* (1), 197-209.

Schmid, T., Bonen, D., Luchene, L., & Linsenmayer, T. (1991). Late events in chondrocyte differentiation: hypertrophy, type X collagen synthesis and matrix calcification. *In vivo (Athens, Greece) , 5* (5), 533-40.

Schulte-Merker, S., van Eeden, F., Halpern, M., Kimmel, C., & Nüsslein-Volhard, C. (1994). no tail (ntl) is the zebrafish homologue of the mouse T (Brachyury) gene. *Development (Cambridge, England) , 120* (4), 1009-15.

Sengle, G., Charbonneau, N., Ono, R., Sasaki, T., Alvarez, J., Keene, D., et al. (2008). Targeting of bone morphogenetic protein growth factor complexes to fibrillin. *The Journal of biological chemistry , 283* (20), 13874-88.

Sengle, G., Ono, R., Sasaki, T., & Sakai, L. (2010, Dec 6). Prodomains of transforming growth factor {beta} (TGF{beta}) superfamily members specify different functions:Extracellular matrix interactions and growth factor bioavailability. *The Journal of biological chemistry* .

Sheppard, D. (2005). Integrin-mediated activation of latent transforming growth factor beta. *Cancer metastasis reviews , 24* (3), 395-402.

Shi, Y., & Massagué, J. (2003). Mechanisms of TGF-beta signaling from cell membrane to the nucleus. *Cell , 113* (6), 685-700.

Smits, P., & Lefebvre, V. (2003). Sox5 and Sox6 are required for notochord extracellular matrix sheath formation, notochord cell survival and development of the nucleus pulposus of intervertebral discs. *Development (Cambridge, England) , 130* (6), 1135-48.

Solnica-Krezel, L., Stemple, D., Mountcastle-Shah, E., Rangini, Z., Neuhauss, S., Malicki, J., et al. (1996). Mutations affecting cell fates and cellular rearrangements during gastrulation in zebrafish. *Development (Cambridge, England) , 123*, 67-80.

Spessotto, P., Cervi, M., Mucignat, M., Mungiguerra, G., Sartoretto, I., Doliana, R., et al. (2003). beta 1 Integrin-dependent cell adhesion to EMILIN-1 is mediated by the gC1q domain. *The Journal of biological chemistry , 278* (8), 6160-7.

Stemple, D. (2005). Structure and function of the notochord: an essential organ for chordate development. *Development (Cambridge, England) , 132* (11), 2503-12.

Sterner-Kock, A. (2002). Disruption of the gene encoding the latent transforming growth factor-beta binding protein 4 (LTBP-4) causes abnormal lung development, cardiomyopathy, and colorectal cancer. *Genes & Development , 16* (17), 2264-2273.

Swiderski, R., & Solursh, M. (1992). Localization of type II collagen, long form alpha 1(IX) collagen, and short form alpha 1(IX) collagen transcripts in the developing chick notochord and axial skeleton. *Developmental dynamics : an official publication of the American Association of Anatomists , 194* (2), 118-27.

Talbot, W., Trevarrow, B., Halpern, M., Melby, A., Farr, G., Postlethwait, J., et al. (1995). A homeobox gene essential for zebrafish notochord development. *Nature , 378* (6553), 150-7.

ten Dijke, P., & Arthur, H. (2007). Extracellular control of TGFbeta signalling in vascular development and disease. *Nature reviews Molecular cell biology , 8* (11), 857-69.

Thisse, C., Thisse, B., Schilling, T., & Postlethwait, J. (1993). Structure of the zebrafish snail1 gene and its expression in wild-type, spadetail and no tail mutant embryos. *Development (Cambridge, England) , 119* (4), 1203-15.

Vaday, G., Hershkoviz, R., Rahat, M., Lahat, N., Cahalon, L., & Lider, O. (2000). Fibronectin-bound TNF-alpha stimulates monocyte matrix metalloproteinase-9 expression and regulates chemotaxis. *Journal of leukocyte biology , 68* (5), 737-47.

Waksman, G., & Herr, A. (1998). New insights into heparin-induced FGF oligomerization. *Nature structural biology , 5* (7), 527-30.

Wang, M., Jin, P., Bumcrot, D., Marigo, V., McMahon, A., Wang, E., et al. (1995). Induction of dopaminergic neuron phenotype in the midbrain by Sonic hedgehog protein. *Nature medicine , 1* (11), 1184-8.

Wang, X., Harris, R., Bayston, L., & Ashe, H. (2008). Type IV collagens regulate BMP signalling in Drosophila. *Nature , 455* (7209), 72-7.

Whittaker, C., Bergeron, K.-F., Whittle, J., Brandhorst, B., Burke, R., & Hynes, R. (2006). The echinoderm adhesome. *Developmental biology , 300* (1), 252-66.

Wolff, C., Roy, S., & Ingham, P. (2003). Multiple muscle cell identities induced by distinct levels and timing of hedgehog activity in the zebrafish embryo. *Current biology : CB , 13* (14), 1169-81.

Yamaguchi, Y., Mann, D., & Ruoslahti, E. (1990). Negative regulation of transforming growth factor-beta by the proteoglycan decorin. *Nature , 346* (6281), 281-4.

Yan, Y., Hatta, K., Riggleman, B., & Postlethwait, J. (1995). Expression of a type II collagen gene in the zebrafish embryonic axis. *Developmental dynamics : an official publication of the American Association of Anatomists , 203* (3), 363-76.

Yayon, A., Klagsbrun, M., Esko, J., Leder, P., & Ornitz, D. (1991). Cell surface, heparin-like molecules are required for binding of basic fibroblast growth factor to its high affinity receptor. *Cell , 64* (4), 841-8.

Zanetti, M., Braghetta, P., Sabatelli, P., Mura, I., Doliana, R., Colombatti, A., et al. (2004). EMILIN-1 deficiency induces elastogenesis and vascular cell defects. *Molecular and cellular biology , 24* (2), 638-50.

Zhao, Q., Eberspaecher, H., Lefebvre, V., & De Crombrugghe, B. (1997). Parallel expression of Sox9 and Col2a1 in cells undergoing chondrogenesis. *Developmental dynamics : an official publication of the American Association of Anatomists , 209* (4), 377-86.

Zhu, Y., Oganesian, A., Keene, D., & Sandell, L. (1999). Type IIA procollagen containing the cysteine-rich amino propeptide is deposited in the extracellular matrix of prechondrogenic tissue and binds to TGF-beta1 and BMP-2. *The Journal of cell biology , 144* (5), 1069-80.

FIGURES

FIGURE 1

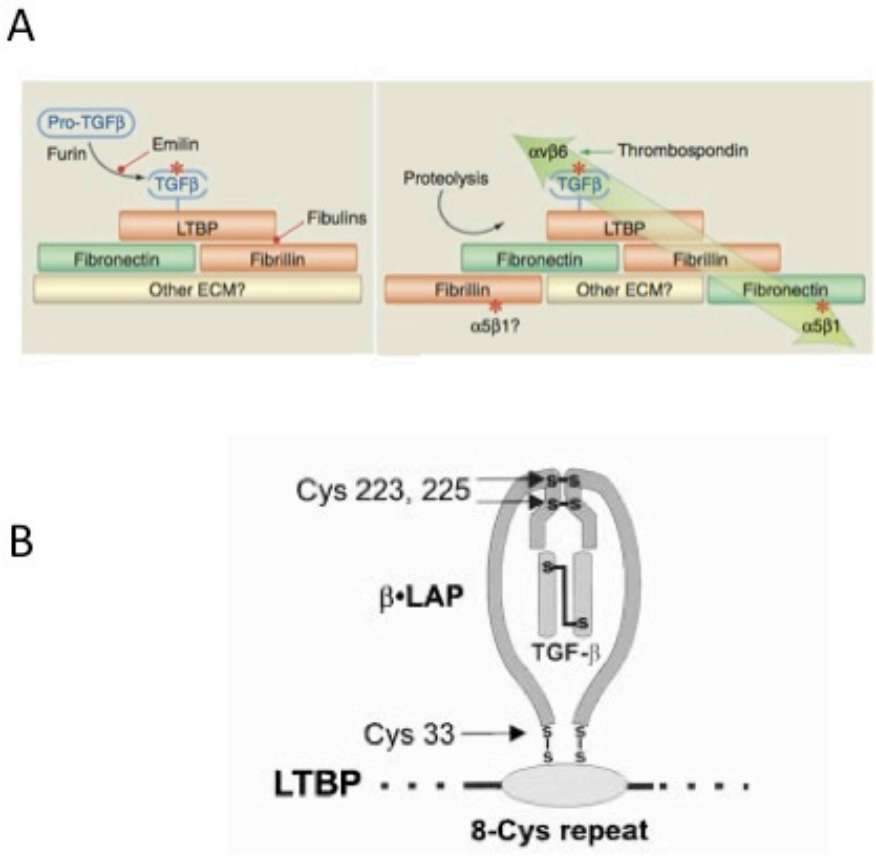

FIGURE 1. Activation of TGF-β and its incorporation in the ECM. A. Left panel. After furin proprotein convertase cleavage (inhibited by Emilin-1), the SLC (Small Latent Complex) binds to LTBP, via disulfide bonding between Cys33 of LAP (Latency Associated Peptide) and a TB domain of LTBP, to form the LLC (Large Latent Complex), in which the TGF-β is inactive (Rifkin 2005; ted Dijke 2007). Right panel. Activation of ECM-bound latent TGF-β. TGF-β can be activated byproteolysis of the ECM proteins and/or of LAP or directly by thrombospondin. TGF-β can also be activated by mechanical strain (large green arrow). **B.** Schematic diagram of the binding between the 8-Cys repeat of LTBP-1 and Cys-33 of TGF-β (**A**, from Hynes, 2009; **B**, from Saharinen et al., 2000).

FIGURE 2 Schematic diagram of the domain structure of Emilin/Multimerin proteins and zebrafish Emilin-3 genes expression pattern. Mammalian (**A**) and zebrafish (**B**) proteins are represented. Emilin-1, Emilin-2, Emilin-3 and Multimerin-2 are duplicated in *Danio rerio*. Conserved cysteine residues are indicated by vertical bars. The asterisk in **B** labels the second cysteine residue of the EMI domain, which is missing in Emilin-3a. SP: signal peptide; EMI: cystein-rich EMI domain; EG: EGF-like domain; LZ: leucine zipper domain; PR: proline rich domain; Col: collagenic domain; CC: charged cluster. Whole-mount in situ hybridization for *emilin3a* and *emilin3b* in zebrafish embryos at 15s, 20s and 24 hpf. Expression of *emilin3a* and *emilin3b* in the notochord, in the chordoneural hinge (asterisk), floor plate and hypochord is shown (**C**). cnh, chordoneural hinge; fl, floorplate; hy, hypochord; no, notochord; yo, yolk sac.

FIGURE 2

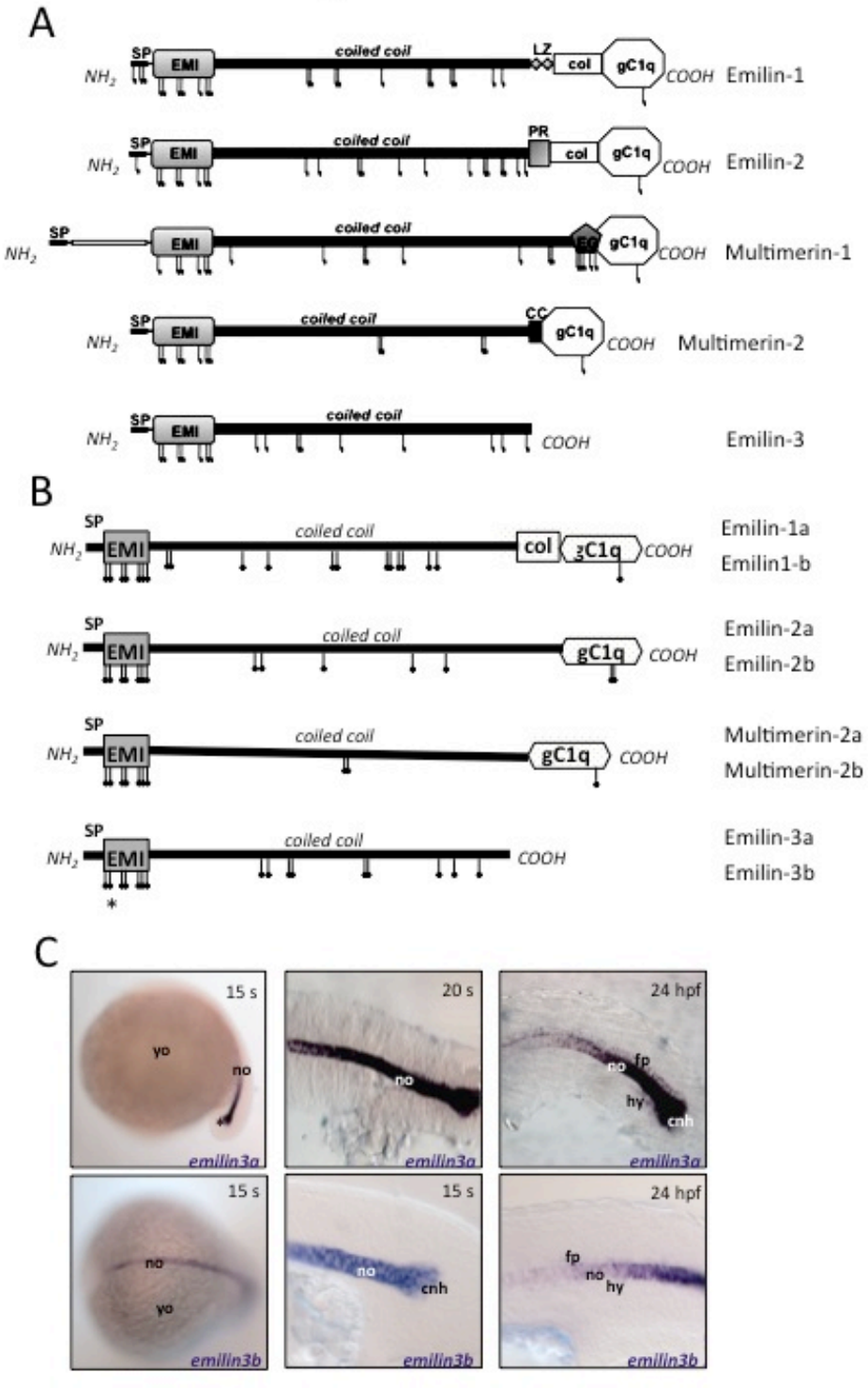
A
SP
EMI
coiled coil
LZ
col
gC1q
NH2
COOH
Emilin-1
PR
Emilin-2
Multimerin-1
CC
Multimerin-2
Emilin-3
B
Emilin-1a
Emilin1-b
Emilin-2a
Emilin-2b
Multimerin-2a
Multimerin-2b
Emilin-3a
Emilin-3b
C
15 s
20 s
24 hpf
yo
no
fp
hy
cnh
emilin3a
emilin3b

FIGURE 3. Aminoacid sequence and coiled coil prediction of murine Emilin-3. Arrow marks the putative signal peptide cleavage site. The black underline indicates the sequence that can be removed by alternative splicing. The EMI domain is highlighted in orange, with the conserved cysteine residues marked by an asterisk. The coiled coil region is highlighted in yellow. Arrowheads indicate four sites predicted to be N-glycosylated (**A**). Predicted coiled coil regions in the C-terminal part of the Emilin-3 sequence as deduced by analysis with Coils software (**B**).

FIGURE 3

A

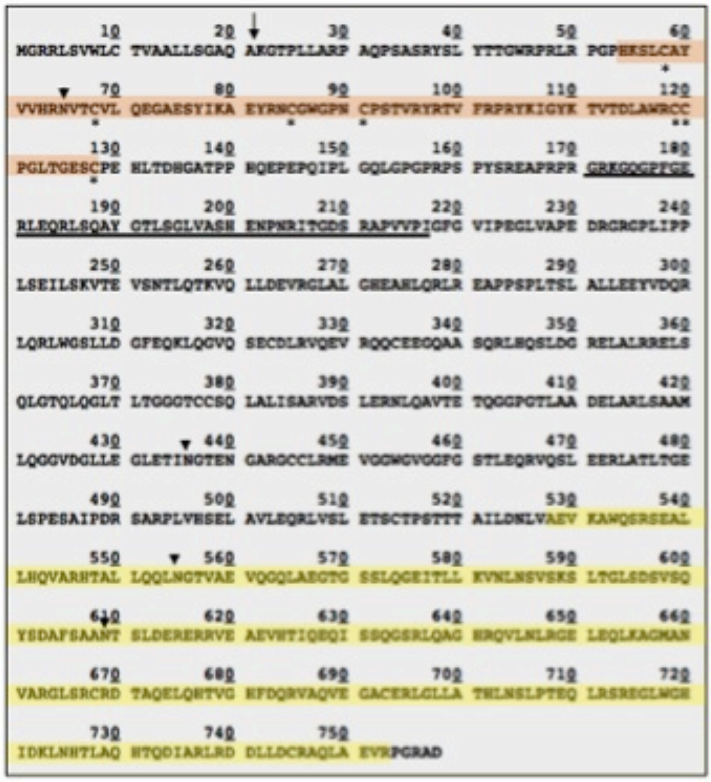
MGRRLSVWLC TVAALLSGAQ AEGTPLLARP AQPSASRYSL YTTGWRPRLR PGPHKSLCAY
VVHRNVTCVL QEGAESYIKA EYRNCGWGPN CPSTVRYRTV FRPRYKIGYK TVTDLAWRCC
PGLTGESCPE HLTDSGATPP SQEPEPQIPL GQLGPGPRPS PYSREAPRPR GRKGGGPFGE
RLEQRLSQAY GTLSGLVASH ENPNRITGDS RAPVVPIGPG VIPEGLVAPE DRGRGPLIPP
LSEILSKVTE VSNTLQTKVQ LLDEVRGLAL GHEAELQRLR EAPPSPLTSL ALLEEYVDQR
LQRLWGSLLD GFEQKLQGVQ SECDLRVQEV RQQCEEGQAA SQRLRQSLDG RELALRRELS
QLGTQLQGLT LTGGGTCCSQ LALISARVDS LERNLQAVTE TQGGPGTLAA DELARLSAAM
LQGGVDGLLE GLETINGTEN GARGCCLRME VGGWGVGGPG STLEQRVQSL EERLATLTGE
LSPESAIPDR SARPLVHSEL AVLEQRLVSL ETSCTPSTTT AILDNLVAEV KAWQERSEAL
LHQVARHTAL LQQLNGTVAE VQGQLAEGTG SSLQGEITLL KVNLNSVSKS LTGLSDSVSQ
YSDAFSAANT SLDERERRVE AEVWTIQEQI SSQGSRLQAG HRQVLNLRGE LEQLKAGMAN
VARGLSRCRD TAQELQRTVG EFDQRVAQVE GACERLGLLA TNLNSLPTEQ LRSREGLWGH
IDKLNHTLAQ HTQDIARLRD DLLDCRAQLA EVRPGRAD

B

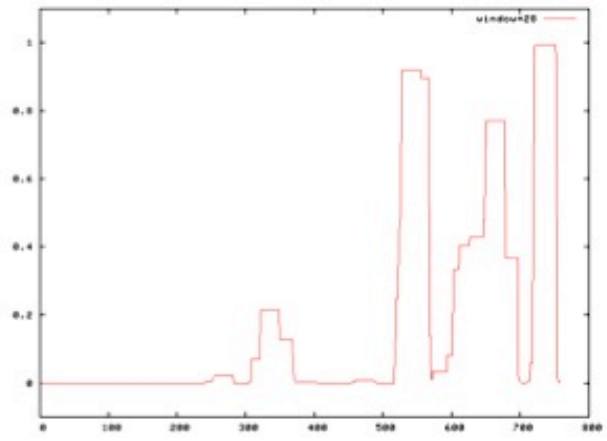
window=20
1
0.8
0.6
0.4
0.2
0
0
100
200
300
400
500
600
700
800

FIGURE 4. Emilin-1 forms a covalent complex with proTGF-β1. A plasmid coding for the full-length Emilin-1 protein was transfected together with proTGF-β1 cDNA into 293T cells, and proteins secreted in the conditioned medium were separated by 3-8% PAGE under non-reducing conditions. The secreted proteins were detected by western blot with antibodies for β1-LAP as indicated, in order to detect the covalent Emilin-1/β1-LAP complex (**A**). Emilin-1 immunoprecipitation of conditioned media followed by western blot for β1-LAP under non-reducing conditions confirmed the formation of a covalent complex and proved that Cys33 of LAP is essential for the binding, while Emilin-1 EMI domain is not (**B**). The transfected cDNAs are indicated above the immunoblots, and the antibodies used are below them. Square brackets indicate proTGF-β dimers and the large β1-LAP/Emilin-1 complex, while the arrow indicates Emilin-1 trimers (T). IP, antibody used for immunoprecipitation; WB, antibody used for western blot.

FIGURE 4

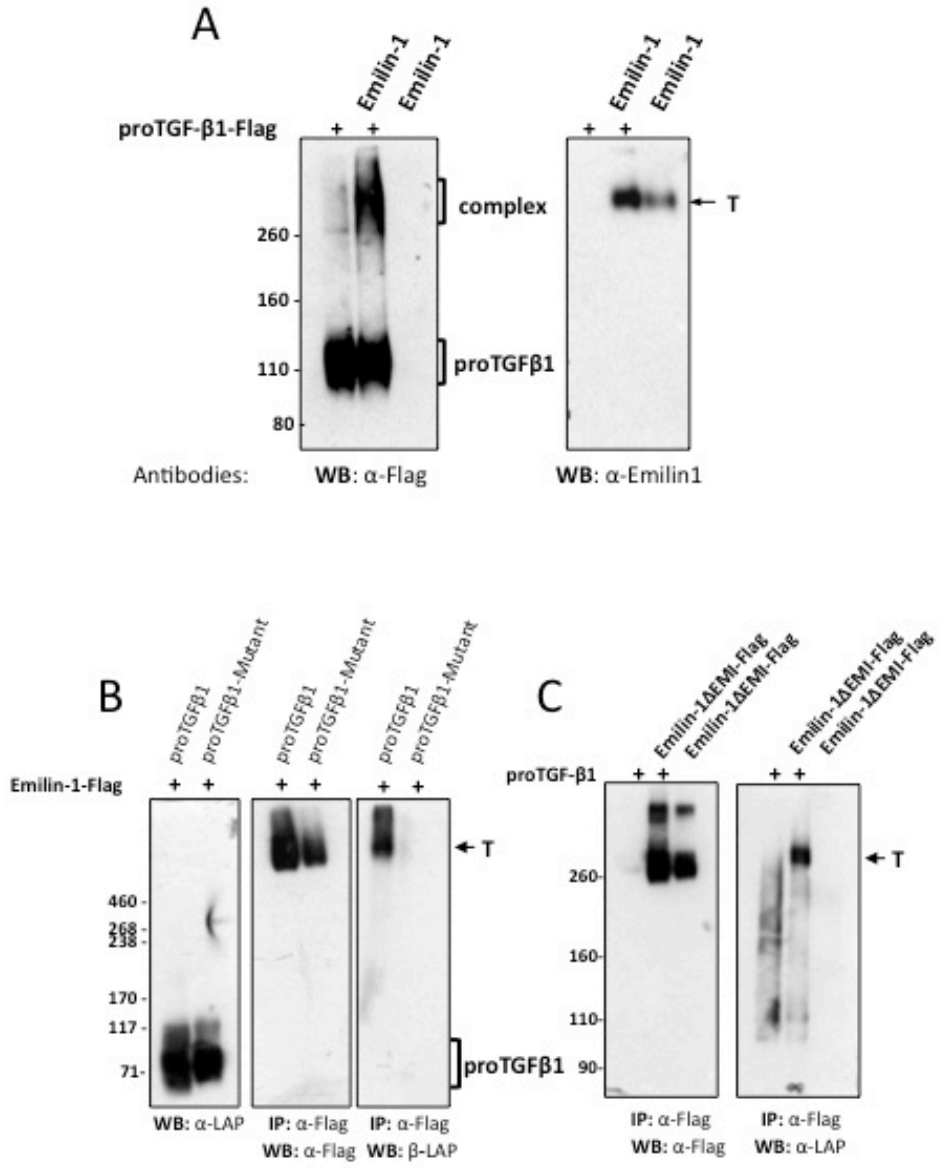
A
Emilin-1
Emilin-1
proTGF-β1-Flag
+ +
complex
260
160
110
80
proTGFβ1
T
Antibodies:
WB: α-Flag
WB: α-Emilin1
B
proTGFβ1
proTGFβ1-Mutant
Emilin-1-Flag
460
268
238
170
117
71
T
proTGFβ1
WB: α-LAP
IP: α-Flag
WB: α-Flag
IP: α-Flag
WB: β-LAP
C
Emilin-1ΔEMI-Flag
proTGF-β1
260
160
110
90
T
proTGFβ1
IP: α-Flag
WB: α-Flag
IP: α-Flag
WB: α-LAP

FIGURE 5. Analysis of *Emilin3* mRNA expression during mouse development and in postnatal and adult mouse tissues. RNA was collected from whole mouse embryos at the indicated developmental stage (**A**) or from postnatal and adult mouse tissues (**B**) and analyzed by semi-quantitative RT-PCR with oligonucleotides designed to detect the two splicing variants differing for 141 base pairs. bp, base pairs. Whole mount *in situ* hybridization of E8.5 and E9.5 embryos reveal *Emilin3* expression in the tail-bud region (arrows in **C**).

FIGURE 5

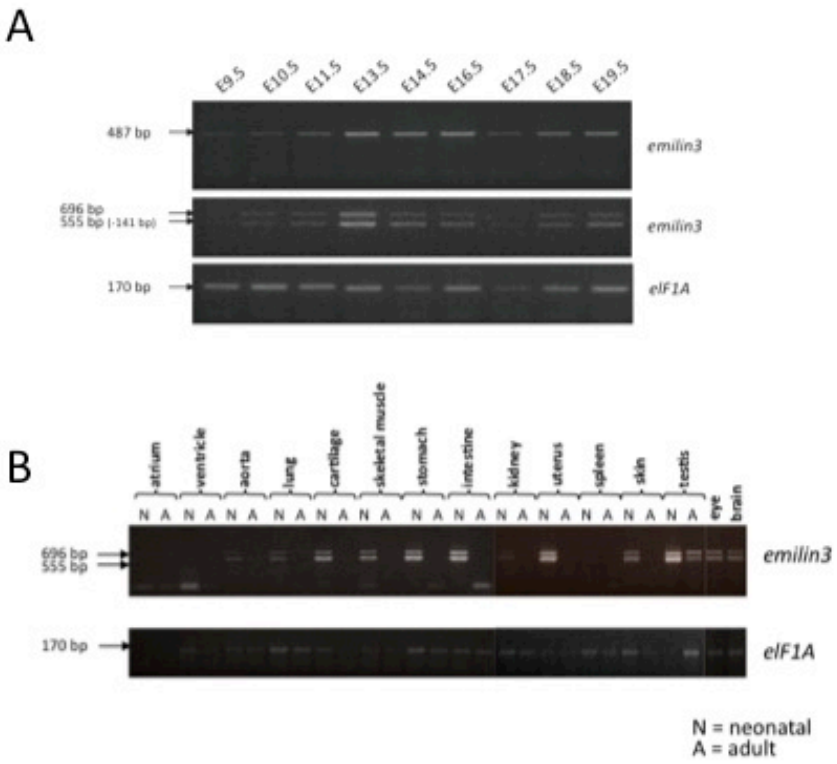
A
E9.5
E10.5
E11.5
E13.5
E14.5
E16.5
E17.5
E18.5
E19.5
487 bp
emilin3
696 bp
555 bp (-141 bp)
emilin3
170 bp
elF1A
B
atrium
ventricle
aorta
lung
cartilage
skeletal muscle
stomach
intestine
kidney
uterus
spleen
skin
testis
eye
brain
N A N A N A N A N A N A N A N A N A N A N A N A N A N A
696 bp
555 bp
emilin3
170 bp
elF1A
N = neonatal
A = adult

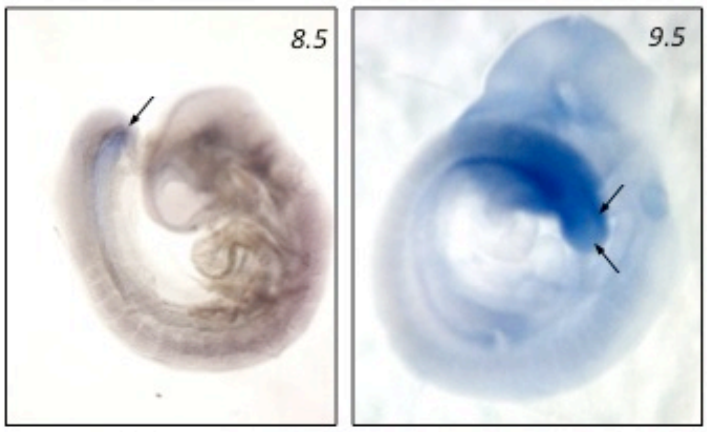
C
8.5
9.5

FIGURE 6. Detection of *Emilin3* mRNA by in situ hybridization on paraffin sections. E11.5 to E14.5 mouse embryos were processed and analyzed by in situ hybridization on paraffin sections with an *Emilin3* antisense probe. Parasagittal sections of whole embryos at E11.5 and E14.5 (A and M). Sagittal and transverse sections show *Emilin3* expression in the ventricular zone of the ventral midbrain (B and C). Expression in the gastrointestinal tract was detected at different developmental stages, and esophagus (D and E) and midgut (F to H) are shown. Expression was found in the subepidermal mesenchyme at the trunk level (I), in gonadal ridges and mesonephric tissue (J, K, L). Eye (N), vibrissae (O) diaphragm and main bronchi (P) were also positive at E14.5. Staining of intervertebral discs (Q), perichondrium of the hindlimb (R) and inner ear (S) are also shown. cm, cephalic mesenchyme; di, diaphragm; gr, gonadal ridge; hl, hindlimb; id, intervertebral discs; ki, kidney; li, liver; ll,lower lip; lu, lung; me, mesencephalon; mg, midgut; mv, mesencephalic vescicle; oe, oesophagus; rb, rib primorida; te, testis; tv, telencephalic vescicle; vb, vertebral bodies; ve, ventricle; III, third ventricle; IV, fourth ventricle. Bar, 50 μm (panels I,P,Q) or 100 μm (other panels).

FIGURE 6

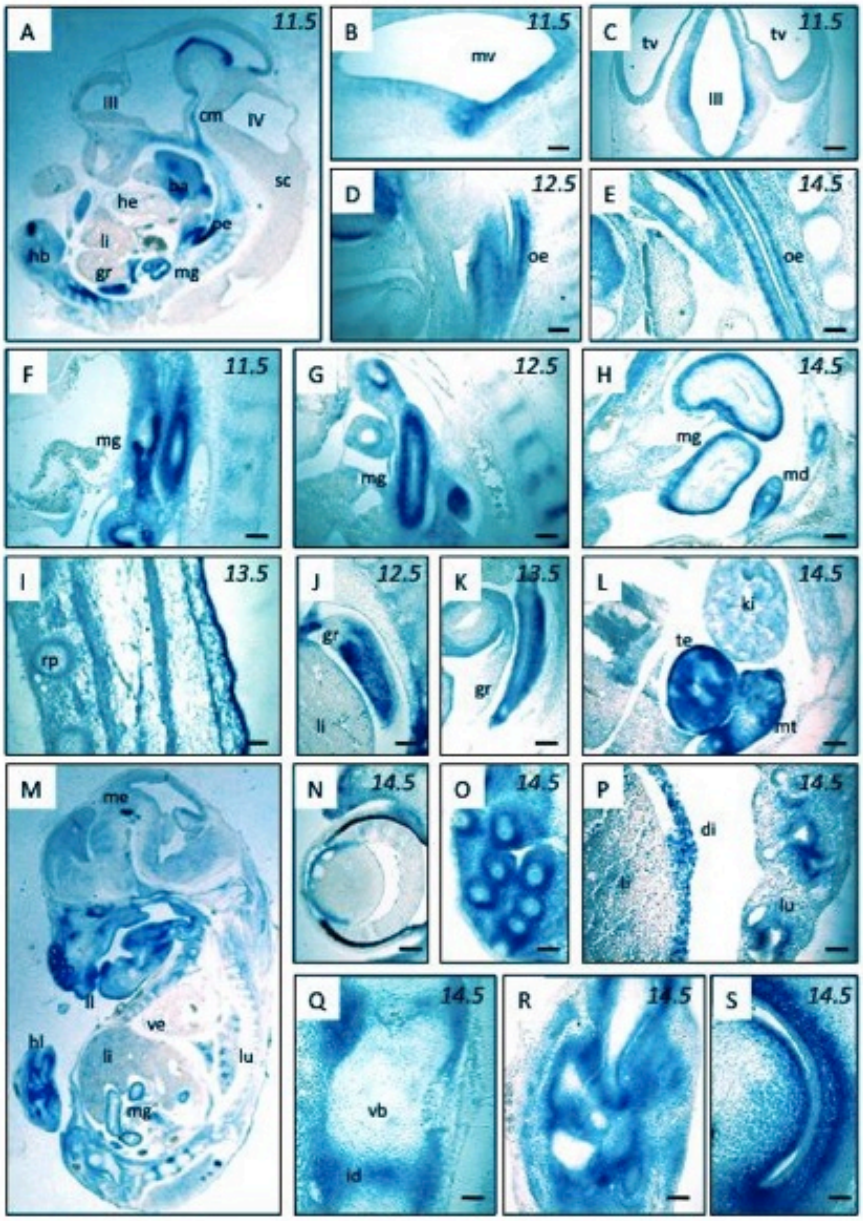
A
11.5
III
om
IV
sc
he
ba
oe
li
hb
gr
mg
B
11.5
mv
C
11.5
tv
tv
III
D
12.5
oe
E
14.5
oe
F
11.5
mg
G
12.5
mg
H
14.5
mg
md
I
13.5
rp
J
12.5
gr
li
K
13.5
gr
L
14.5
ki
te
mt
M
me
ll
ve
hl
li
lu
mg
N
14.5
O
14.5
P
14.5
di
li
lu
Q
14.5
vb
id
R
14.5
S
14.5

FIGURE 7. Emilin-3L and Emilin-3s are expressed in the cell layer but not in the conditioned medium of transfected cells. HEK293T cells were transfected with the indicated expression constructs; the cell layers and conditioned media were analyzed under reducing or non-reducing conditions using the specified antibodies. While both Emilin-1 and Emilin-2 recombinant proteins were detected in the conditioned media of transfected cells (**B**), no Emilin-3 could be found in this fraction (**A** and **B**). The mobility of Emilin-3 under non-reducing conditions suggests homotrimers formation (**A**). No protein was detected in cells transfected with the empty vector. The transfected cDNAs are indicated above the immunoblots. C, cell layer; M, conditioned medium; EV, empty vector; T, trimers. D, dimers. HEK293T cells were cotransfected with the Emilin-3L construct and the reporter plasmid D1ER. The majority of Emilin-3 protein, as detected by indirect immunofluorescence, co-localized with D1ER in the endoplasmic reticulum. Furthermore, some Emilin-3 was detected outside cells and deposited on the coverslip, indicating that Emilin-3 is secreted by transfected cells (**C**) Scale bar: 10 μm.

FIGURE 7

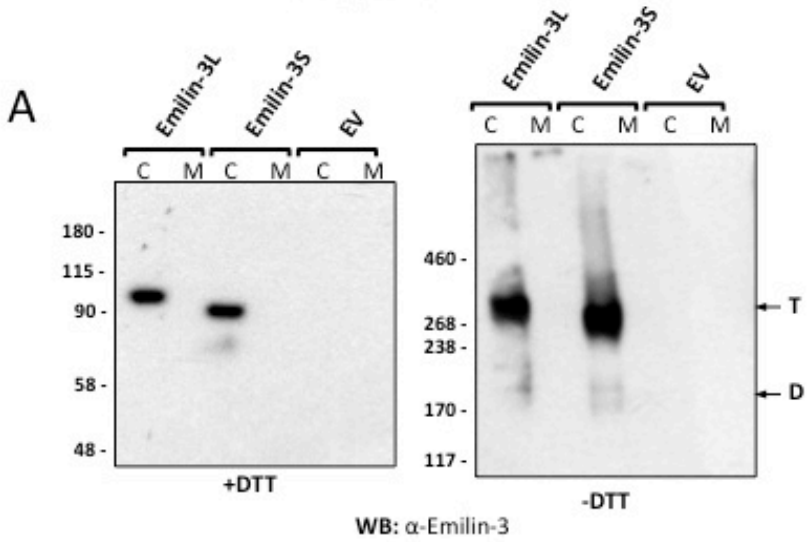
A
Emilin-3L
Emilin-3S
EV
C M C M C M
180 -
115 -
90 -
58 -
48 -
+DTT
Emilin-3L
Emilin-3S
EV
C M C M C M
460 -
268 -
238 -
170 -
117 -
T
D
-DTT
WB: α-Emilin-3

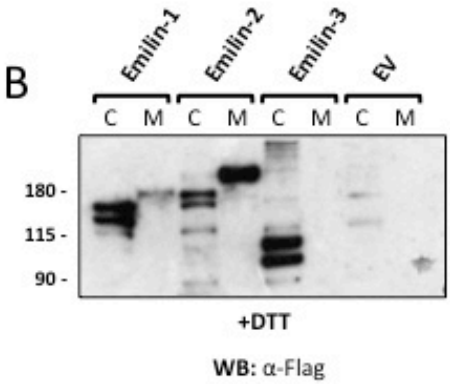
B
Emilin-1
Emilin-2
Emilin-3
EV
C M C M C M C M
180 -
115 -
90 -
+DTT
WB: α-Flag

C

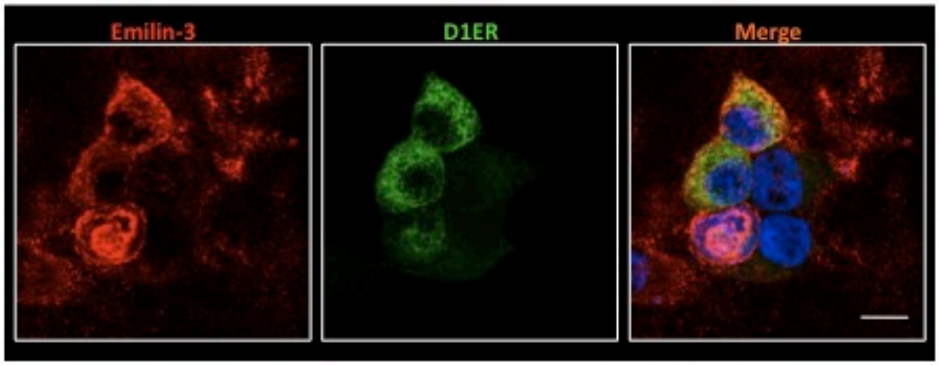
Emilin-3
D1ER
Merge

FIGURE 8. Emilin-3 is associated with the ECM and solubilized by heparin. After transfection with the indicated constructs, HEK293T cells were harvested in cold RIPA buffer and the insoluble material attached to the culture dish was extracted in Laemmli sample buffer at 90°C. The obtained material was analyzed by western blot with an antibody against Emilin-3. The protein was not detected in the conditioned medium but it was abundant in the ECM extract (**A**). After the addition of soluble heparin to the culture system, Emilin-3 was released from the ECM and appeared in the medium (**A**, lower blot). The same observation was confirmed by immunofluorescence experiments. After heparin treatment, the amount of extracellular Emilin-3 deposited on the coverslip was reduced (**B**). C, cell layer; ECM, ECM extract; M, conditioned medium; EV, empty vector. Scale bar: 20 μm

FIGURE 8

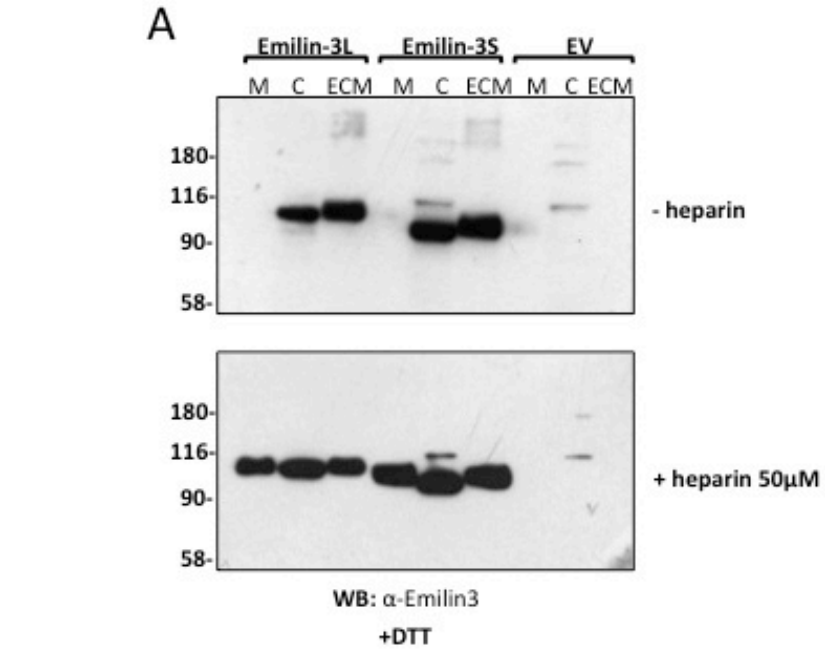
A
Emilin-3L
Emilin-3S
EV
M C ECM M C ECM M C ECM
180-
116-
90-
58-
- heparin
180-
116-
90-
58-
+ heparin 50µM
WB: α-Emilin3
+DTT

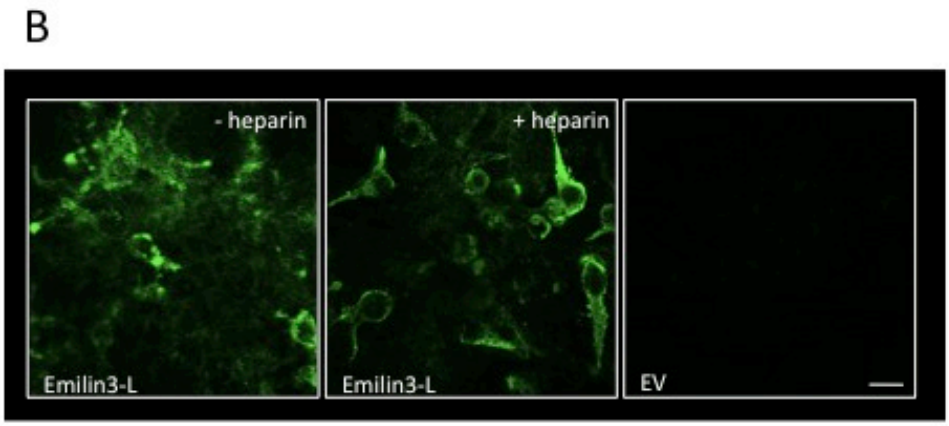
B
- heparin
+ heparin
Emilin3-L
Emilin3-L
EV

FIGURE 9. Emilin-3 binds to heparin through its EMI domain. Cell lysates of transfected HEK293T cells were immunoprecipitated with agarose beads conjugated with heparin. After three washes in lysis buffer, immunoprecipitates were eluted with buffers containing increasing NaCl concentrations. While Emilin-3L and Emilin-3S bind heparin with high affinity, Emilin-3ΔEMI could not be immunoprecipitated, suggesting that the EMI domain is the heparin binding domain of the protein (**A**). C, total cell lysate; -, unconjugated beads; numbers represent NaCl molarity of washing solutions. In agreement with this, Emilin-3ΔEMI is easily detected in the conditioned medium of transfected 293T cells, probably as a consequence of diminished affinity for the ECM (**B**). C, cell layer; ECM, ECM extract; M, conditioned medium; EV, empty vector.

FIGURE 9

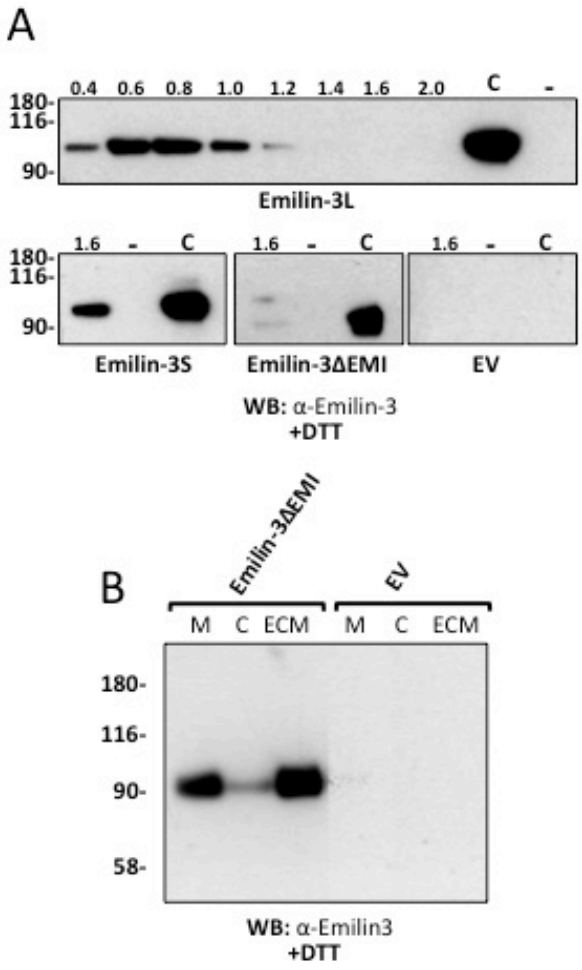
A
0.4 0.6 0.8 1.0 1.2 1.4 1.6 2.0 C -
180-
116-
90-
Emilin-3L
1.6 - C 1.6 - C 1.6 - C
180-
116-
90-
Emilin-3S
Emilin-3ΔEMI
EV
WB: α-Emilin-3
+DTT
B
Emilin-3ΔEMI
EV
M C ECM M C ECM
180-
116-
90-
58-
WB: α-Emilin3
+DTT

FIGURE 10. Analysis of trimer and multimer formation of Emilins. HEK293T cells were transfected with the indicated plasmids, harvested and analyzed by western blots under reducing or non-reducing conditions. All the tested recombinant proteins formed disulfide-linked homotrimers under non-reducing conditions in a 3-8 % gradient acrylamide gel (**A**). Analysis by agarose-acrylamide composite gels revelead that the gC1q domain is dispensable for high molecular weight aggregates formation and suggested a role for the EMI domain in the formation of higher order aggregates (**B**).

FIGURE 10

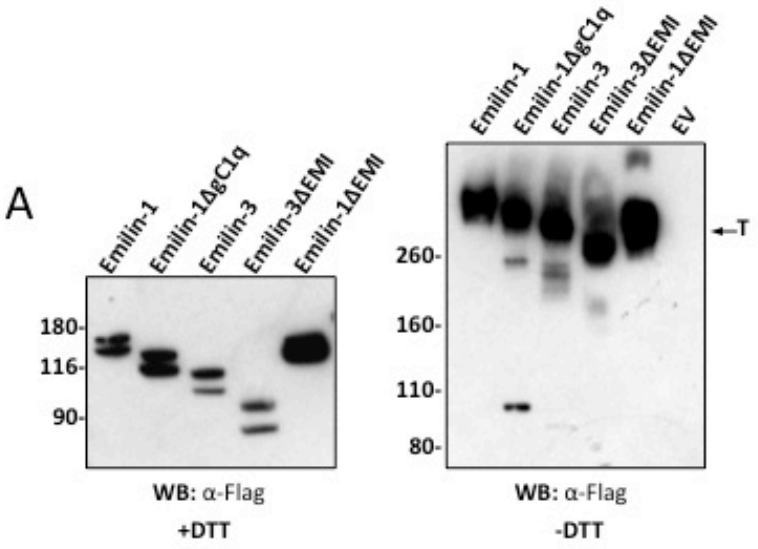
A
Emilin-1
Emilin-1ΔgC1q
Emilin-3
Emilin-3ΔEMI
Emilin-1ΔEMI
EV
180-
116-
90-
260-
160-
110-
80-
←T
WB: α-Flag
+DTT
WB: α-Flag
-DTT

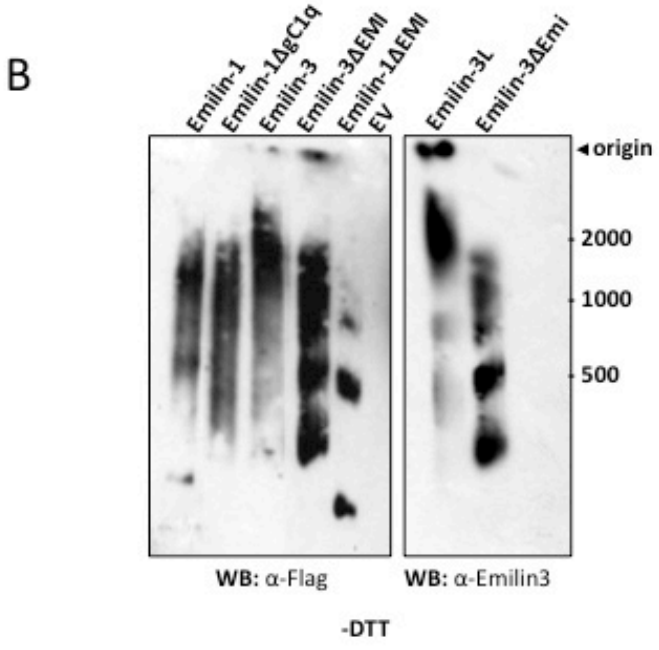
B
Emilin-1
Emilin-1ΔgC1q
Emilin-3
Emilin-3ΔEMI
Emilin-1ΔEMI
EV
Emilin-3L
Emilin-3ΔEmi
◂origin
2000
1000
500
WB: α-Flag
WB: α-Emilin3
-DTT

FIGURE 11

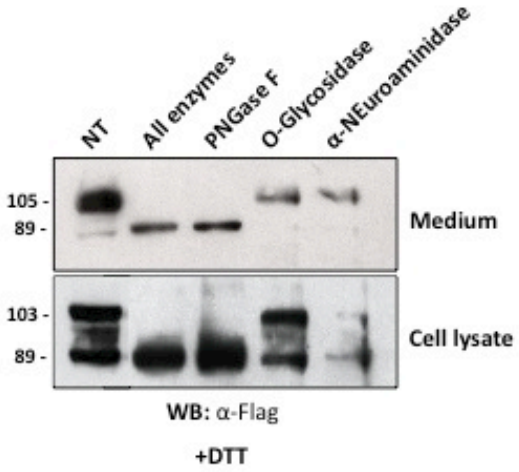

FIGURE 11. Emilin-3 is N-glycosylated. HEK293T cells were transfected with a Flag-tagged construct of Emilin-3L. Cell lysate and concentrated conditioned medium were treated with the indicated enzymes and analyzed by western blot. Only the treatment with the N-glycosidase F displayed an effect, indicating that Emilin-3 udergoes N-glycosylation.

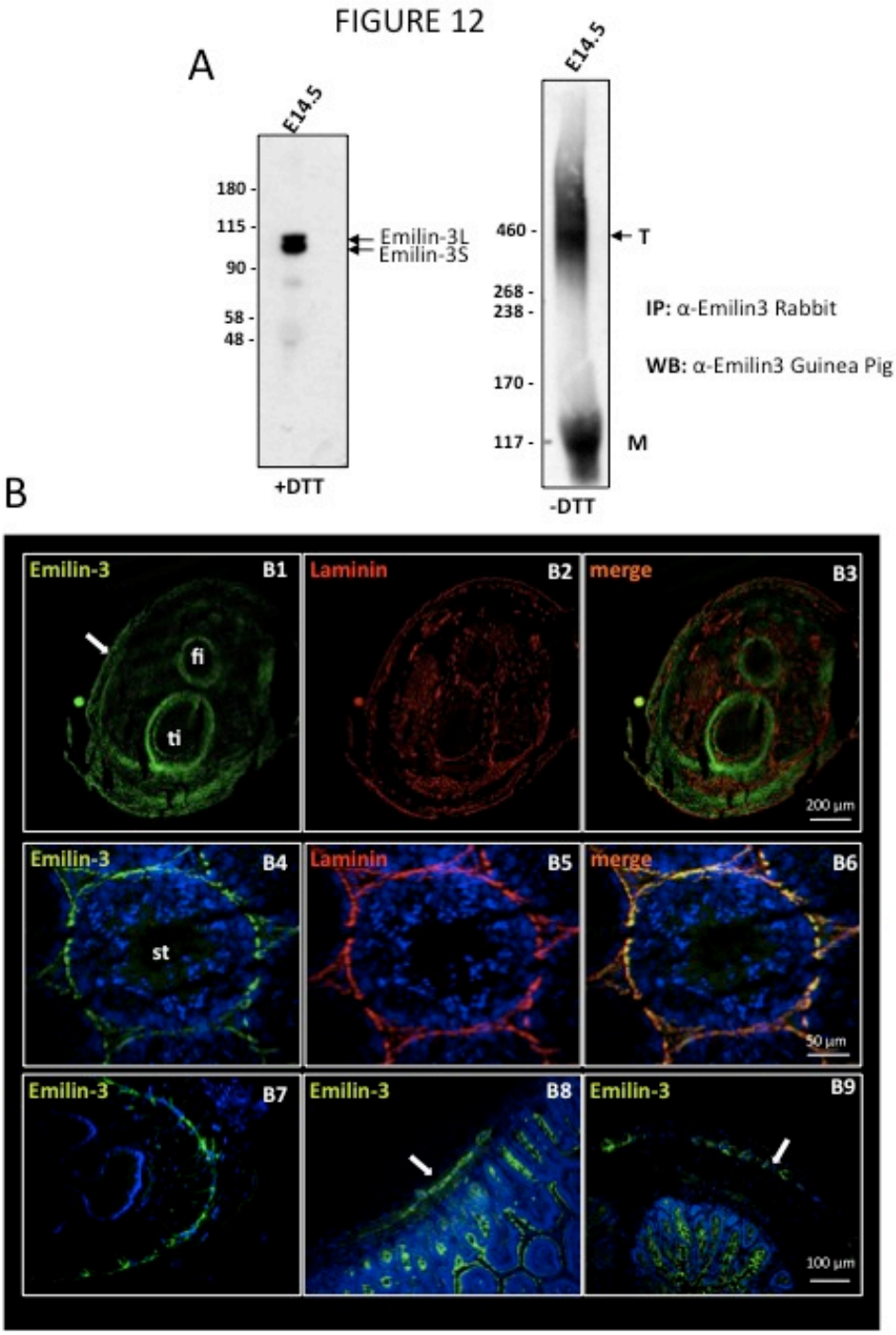

FIGURE 12. Emilin-3 protein in embryonic and adult mouse tissues. Immunoprecipitation with two Emilin-3 specific antibodies detected both Emilin-3L and Emilin-3S in a whole embryo extract (**A**). Immunolocalization of Emilin-3 in E14.5 hindlimb transverse sections (B1-3) showing a strong deposition in the perichondrium of developing bones and in subepidermal mesenchyme (arrow in B1). Emilin-3 colocalizes with laminin in the basament membrane of seminiferous tubule in adult testis (B4-6). Emilin-3 distribution around myoenteric plexus of the esophagus, ileum and colon (B7-9, respectively). fi, fibula; st, seminiferous tubules; ti: tibia; arrows in B8 and B9 mark the specific staining of the myoenteric plexus.

FIGURE 13. Emilin-3 interacts with Emilin-1

Double immunostaining of Emilin-1 and Emilin-3 in embryonic tissues showed partial overlapping distribution of the two proteins. Transverse sections of E14.5 forelimb at the level of metacarpal bones (**A**). White box in the upper panel indicates region magnified in the panels below. Transverse sections of E14.5 midgut (**B**). In both tissues the Emilin-3 staining overlapped completely with Emilin-1. Immunoprecipitation of transfected HEK293T cells demonstrated a physical interaction between Emilin-3 and Emilin-1 that is independent from the EMI and the gC1q domain (**C,** and not shown).

FIGURE 13

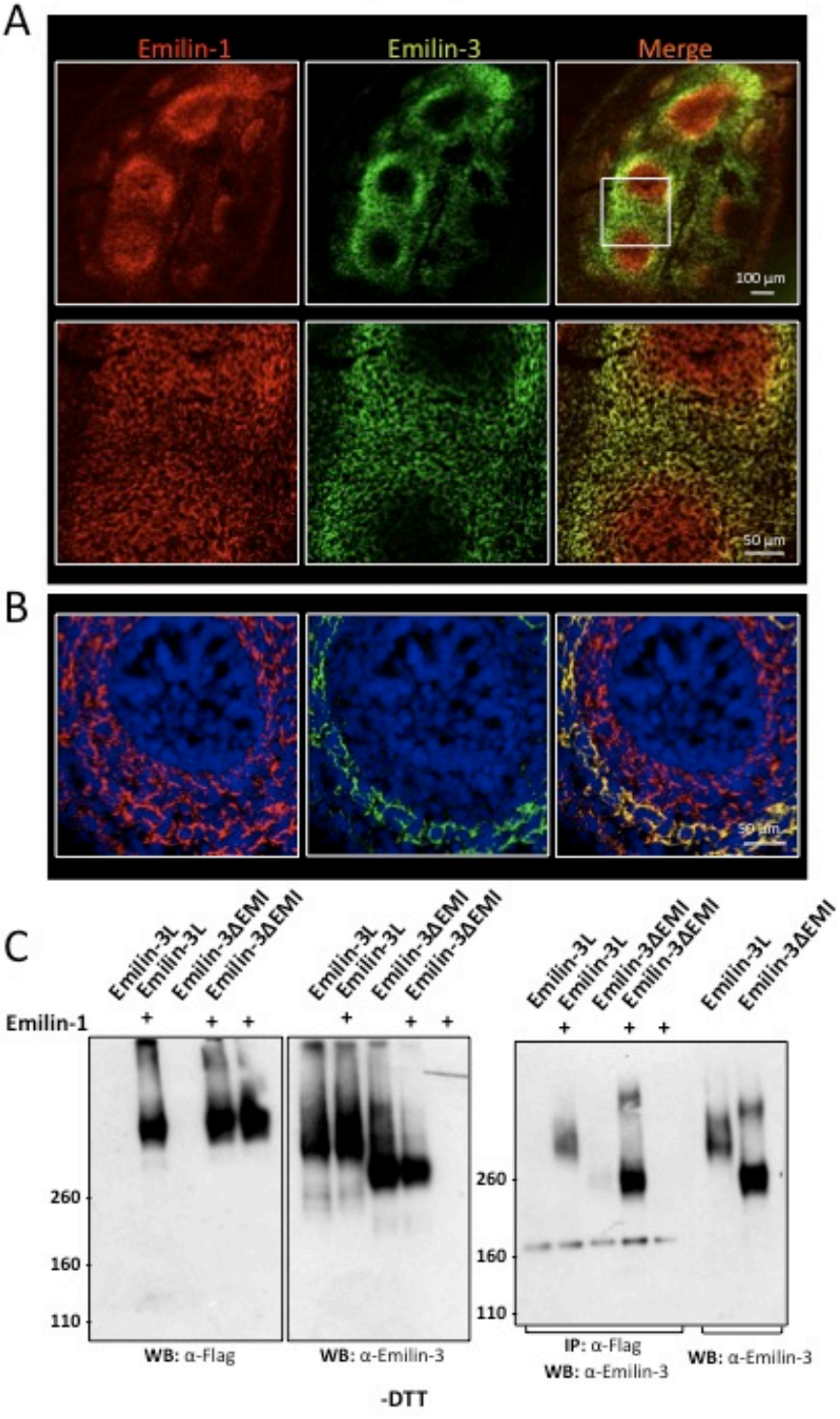
A
Emilin-1
Emilin-3
Merge
100 µm
50 µm
B
50 µm
C
Emilin-3L
Emilin-3L
Emilin-3ΔEMI
Emilin-3ΔEMI
Emilin-1
+
+
+
260
160
110
WB: α-Flag
WB: α-Emilin-3
-DTT
IP: α-Flag
WB: α-Emilin-3

FIGURE 14. Emilin-3 is localized in the notochordal basament membrane during early zebrafish development. Lateral views of the distribution of Emilin-3 protein in zebrafish embryos, by immunofluorescence with anti-Emilin-3 polyclonal antibody on 20 and 24 hpf wild-type embryos. Emilin-3 was detected in the notochord of 20 hpf embryos, co-localizing in part with collagen II (**A**). At 24 hpf, marked labeling for Emilin-3 is detected in a thin layer surrounding the notochord (**B**). Co-immuno staining with collagen II confirmed that at 24 hpf Emilin-3 is localized in the peri-notochordal ECM sheath (**C**). no: notochord.

FIGURE 14

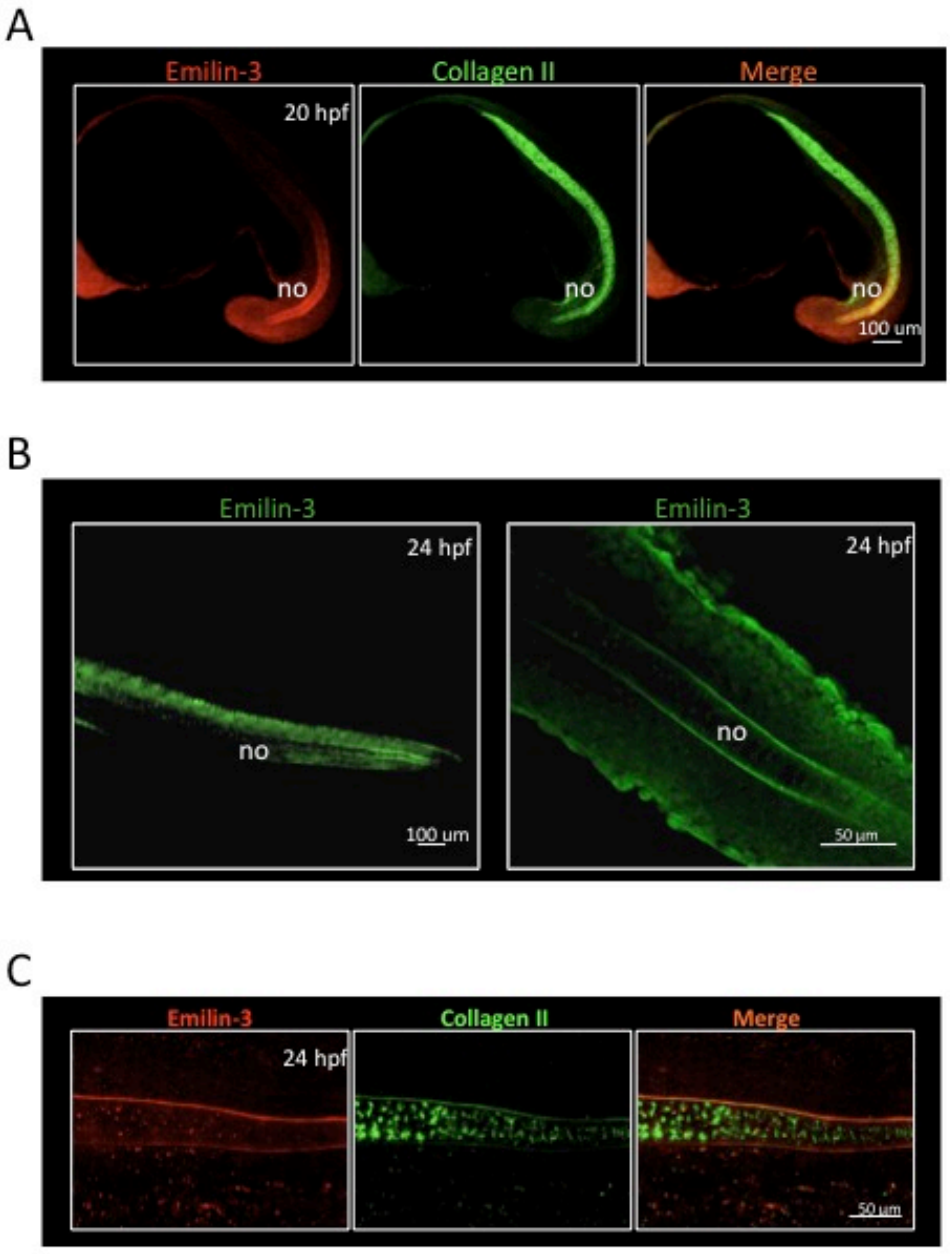
A
Emilin-3
Collagen II
Merge
20 hpf
no
no
no
100 um
B
Emilin-3
Emilin-3
24 hpf
24 hpf
no
no
100 um
50 µm
C
Emilin-3
Collagen II
Merge
24 hpf
50 µm

FIGURE 15. Injection of morpholinos blocking *emilin3a* and *emilin3b* RNA splicing cause several alterations during zebrafish development. To knockdown both zebrafish Emilin-3 genes, one- or two-cell stage embryos were injected either with morpholinos directed against splice sites of *emilin3a/3b* or with control morpholinos. At 30 hpf, *emilin3a/3b* morphant embryos were shorter than controls (arrow), displayed a ventral curvature and a striking distortion of the notochord structure (arrowheads) (**A**). The penetrance of the observed phenotype was dependent from the injected dose. The injected dose of morpholino is indicated in ng/embryo as a sum of *emilin3a* and *emilin3* morpholinos (**B**). Embryos injected with control morpholinos were undistinguishable from wild-type. Embryos were classified in three groups: WT, when no defects were observed; other defects, when no specific alterations were detected; notochord defects: embryos displaing a kinked notochord.

FIGURE 15

A

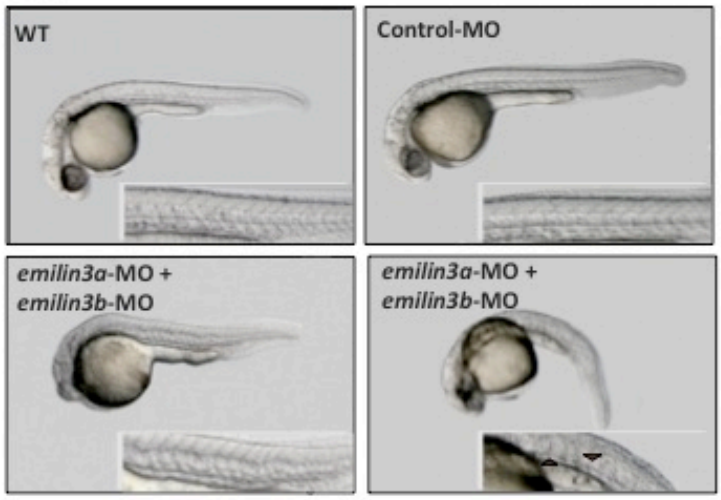
30 hpf
WT
Control-MO
emilin3a-MO +
emilin3b-MO
emilin3a-MO +
emilin3b-MO

B

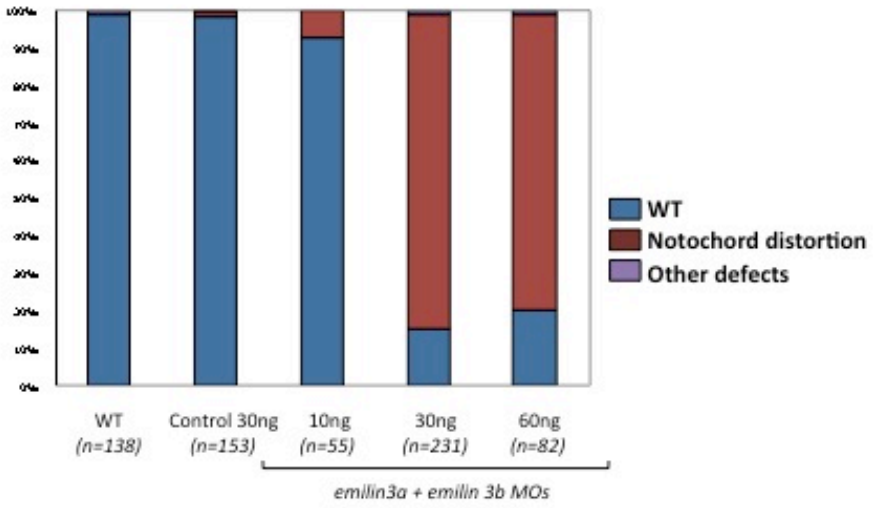
WT
Notochord distortion
Other defects
WT
(n=138)
Control 30ng
(n=153)
10ng
(n=55)
30ng
(n=231)
60ng
(n=82)
emilin3a + emilin 3b MOs

FIGURE 16

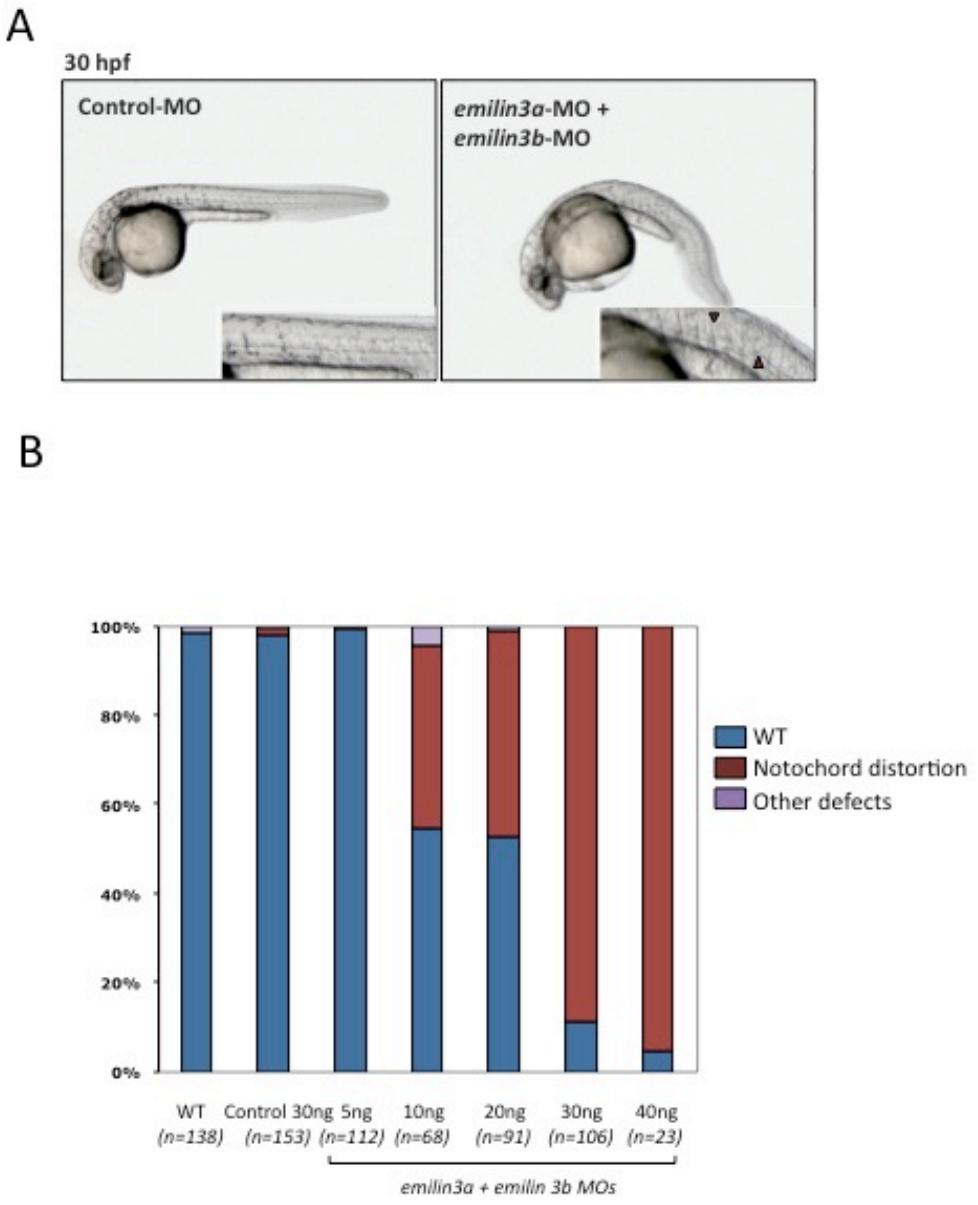

FIGURE 16. Injection of morpholinos blocking *emilin3a* and *emilin3b* translation recapitulates the knockdown phenotype. One- or two-cell stage zebrafish embryos were injected either with morpholinos directed against the translation initiation site of *emilin3a/3b* or with control morpholinos. At 30 hpf, *emilin3a/3b* morphant embryos displayed the same phenotype (Arrowheads) observed for embryos injected with splicing-blocking morpholinos (**A**). Again, *emilin3a/3b* morpholino effects were dose-dependent (**B**). Embryos were divided in three phenotypic groups as in fig. 15.

FIGURE 17

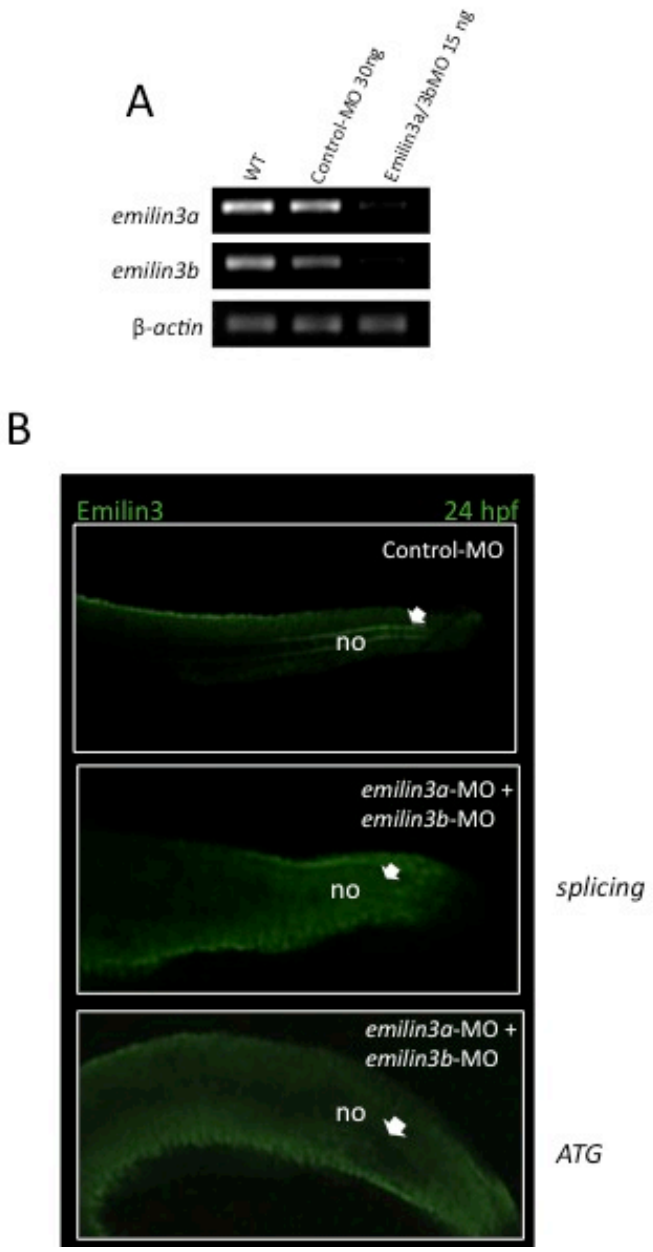

FIGURE 17: Analysis of the efficacy of *emilin3a/3b* knockdown strategies. Total RNA was extracted at the 24 hpf stage from wild-type zebrafish embryos, embryos injected with control morpholinos and embryos injected with *emilin3a/3b* splice-blocking morpholinos, and analyzed by RT-PCR for *emilin3a* and *-3b* mRNAs. *emilin3a/3b* morphant embryos showed almost no mRNAs for both transcripts, suggesting that retention of the first intron causes transcript degradation (**A**). Leteral views of whole mount immunofluorescence for Emilin-3, showing absence of the protein from the notochord sheath of *emilin3a/3b* morphant embryos at 24 hpf while the protein is present in control embryos (arrow in **B**). Splicing, splice-blocking morpholinos; ATG, translational blocking morpholino. no, notochord.

FIGURE 18

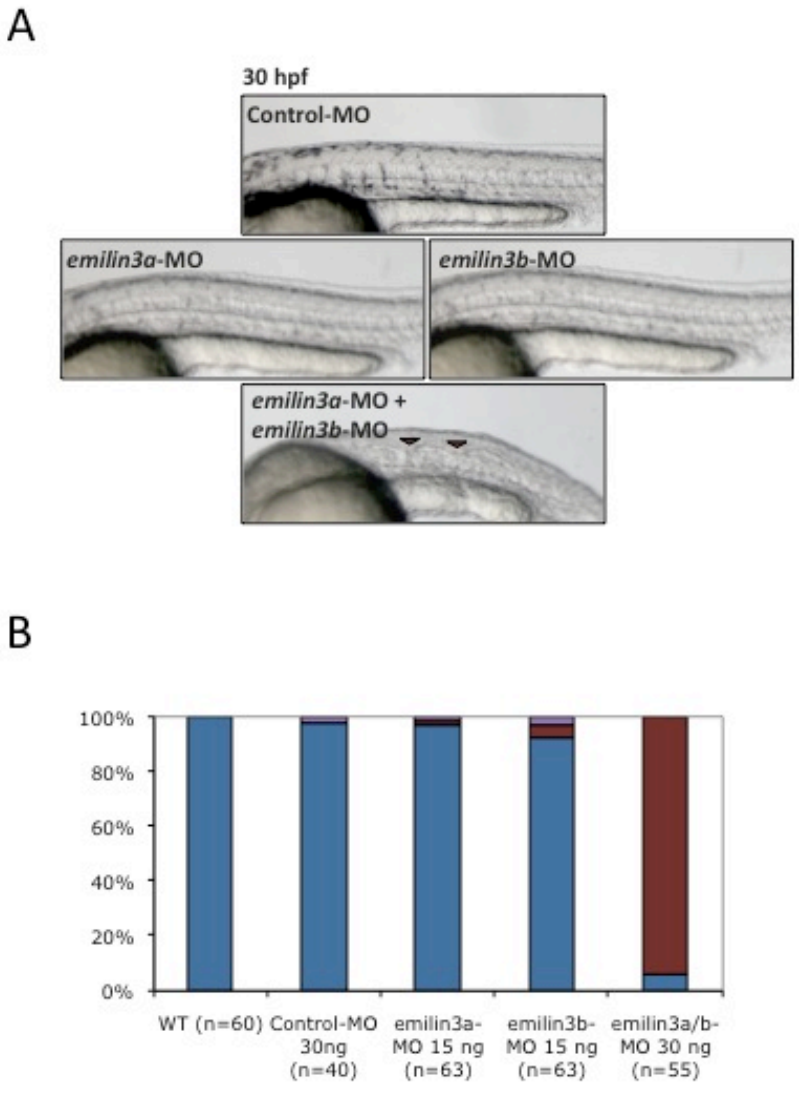

FIGURE 18. Single *emilin3a* or *emilin3b* knockdown does not cause any phenotype. Injection of one- or two-cell-stage zebrafish embryos with single morpholino directed against either *emilin3a* or *emilin3b* did not cause any overt notochord phenotype while the co-injection of *emilin3a* and *-3b* oligonucleotides caused the kinking of the notochord (arrowheads in **A**). Embryos were divided in three groups as in fig. 15 (**B**).

FIGURE 19

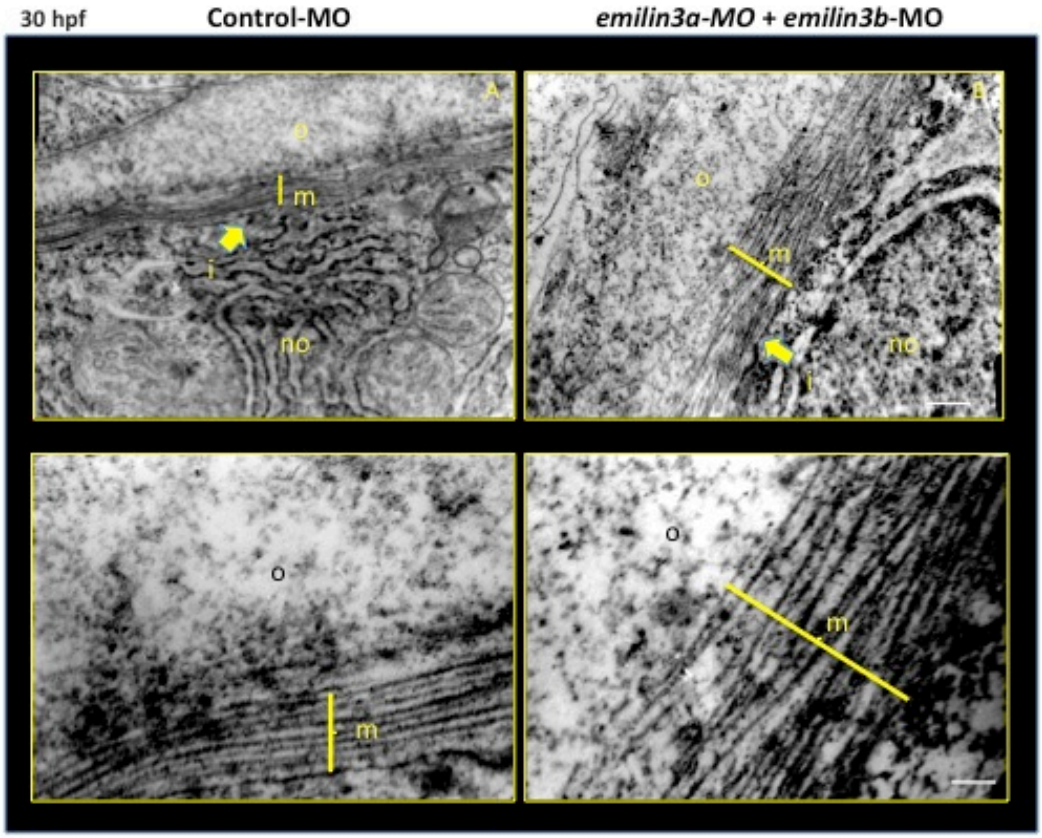

FIGURE 19. Electron microscopy of the notochord of Emilin-3 double morphant embryos, showing disorganization of the notochordal ECM sheath. Transverse sections of *emilin3a/3b* double morphant zebrafish embryos at 30 hpf were analyzed by transmission electron microscopy. The three layers of the notochordal sheath are conserved, but longitudinal fibers of the middle layer are disarranged and interrupted in morphant embryos. Moreover, the middle layer appears thicker than normal. Embryos injected with control morpholinos display normal structure of notochordal sheath. no: notochord; i: inner and arrow; m: middle; o: outer. bars correspond to 680 and 210 nm

FIGURE 20

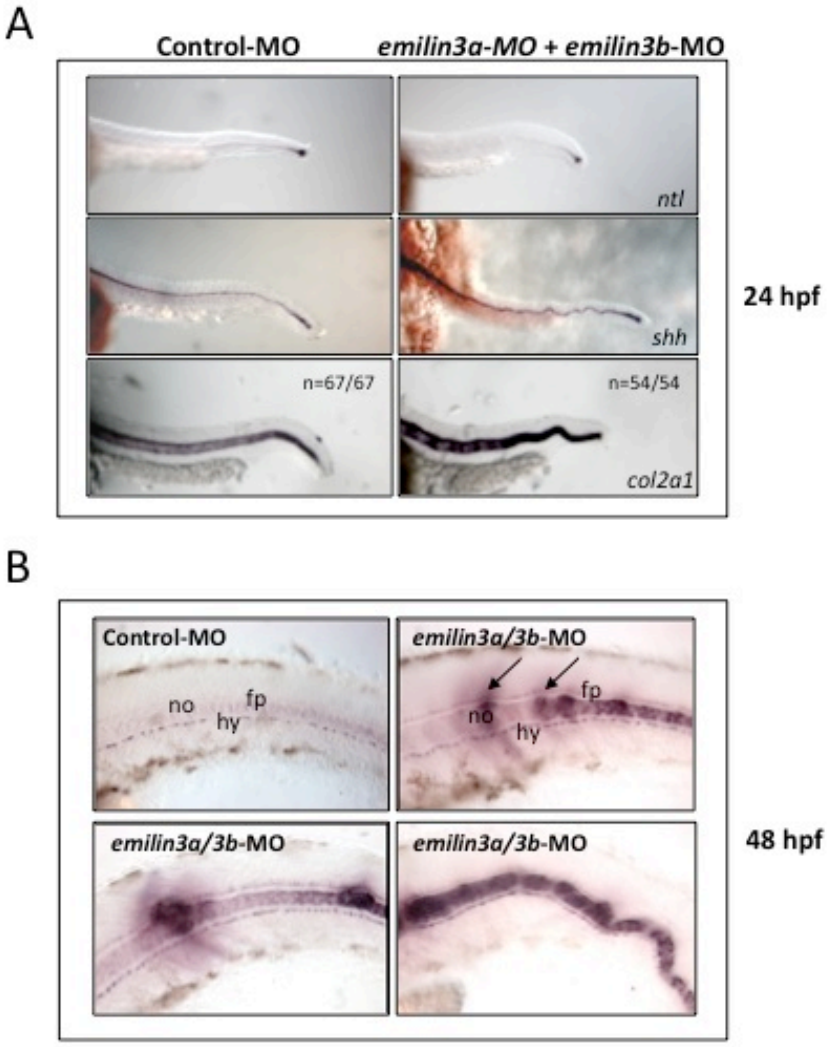

FIGURE 20. Upregulation of *col2a1* gene in Emilin-3 double morphant embryos. Control and morphant zebrafish embryos at 24 hpf were probed for *ntl*, *shh* and *col2a1* expression (**A**). Upregulation of *col2a1* is evident in the notochord of double morphant embryos. At 48 hpf, c*ol2a1* is expressed in control embryos only by cells of the hypochord and of the floorplate, while in *emilin3a/3b* morphant embryos c*ol2a1* is ectopically expressed by vacuolated notochordal cells, around some blood vessesls (not shown) and in the intersomitic spaces (arrows in **B**). *fl:* floorplate; *hy*: hypochord; *no:* notochord.

FIGURE 21

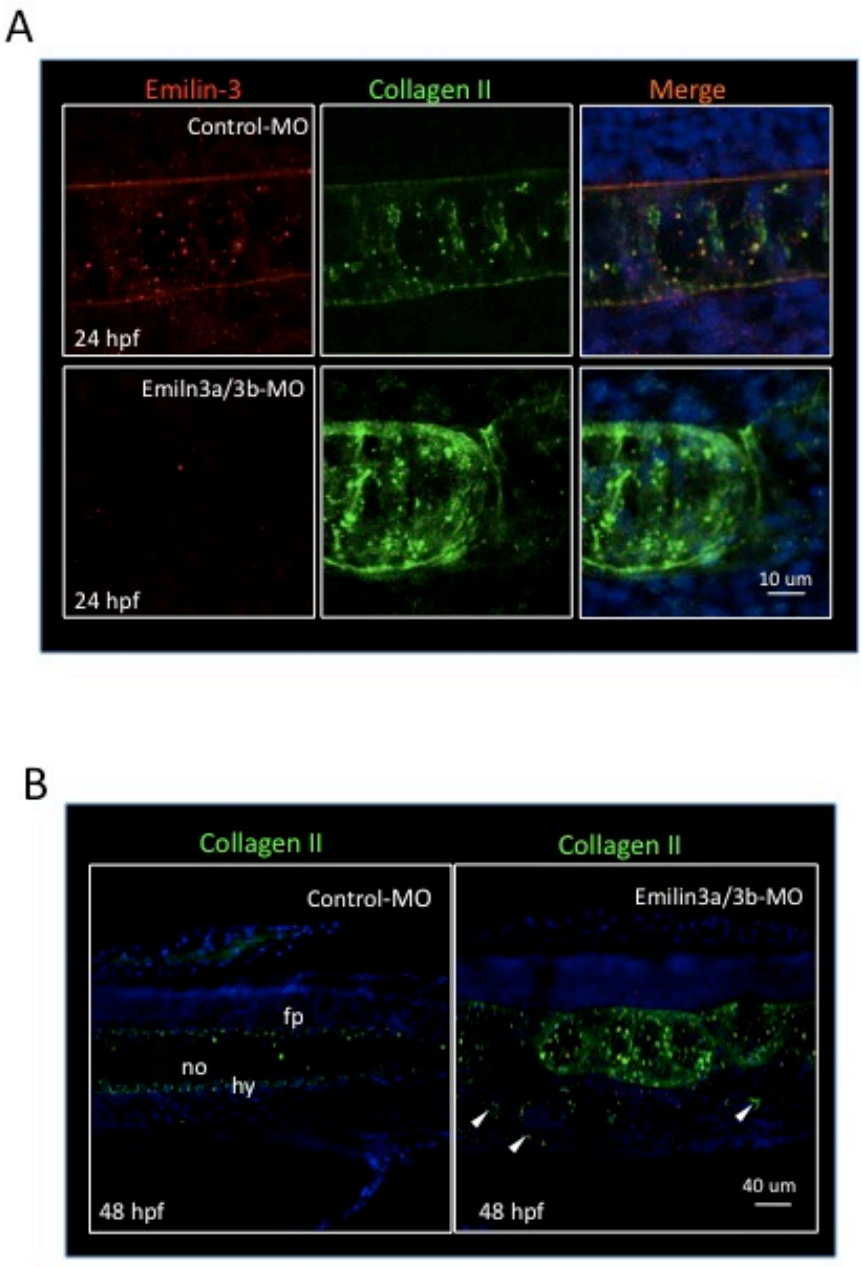

FIGURE 21: Collagen II is upregulated in the notochord of Emilin-3 double morphant embryos. Lateral views of whole mount immunostaining of zebrafish embryos injected with either control morpholino or *emilin3a/3b* morpholino. Increased deposition of collagen II was detected at 24 **(A)** and 48 hpf **(B)** in the notochord of *emilin3a/3b* double morphant embryos. Arrowheads point to some cells with ectopic production of collagen II. *fl:* floorplate; *hy*: hypochord; *no:* notochord.

FIGURE 22. Emilin-3 double morphant embryos are sensitized to lysyl oxidase inhibition. Lysyl oxidase activity is essential for normal notochord development, and treatment of wild-type (WT) zebrafish embryos with the lysyl oxidase the inhibitor β-aminopropionitrile (β-APN) induces the formation of a wavy notochord similar to that observed in Emilin-3 double morphant embryos (**A**). Combined treatment with subtoxic doses of β-APN and Emilin-3 splice-blocking morpholinos cause notochord alteration while treatment with DMSO had no effects (arrowheads in **B**, **C**).

FIGURE 22

A

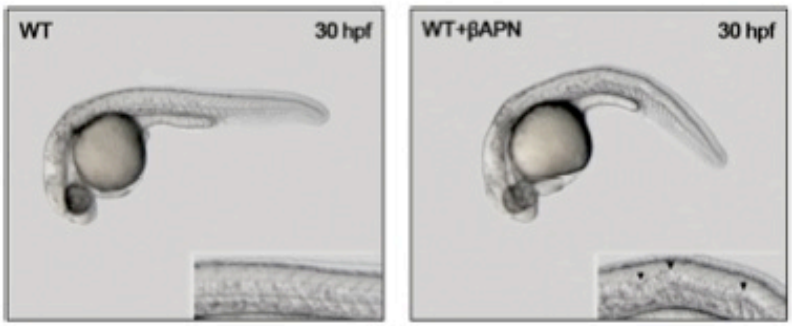

B

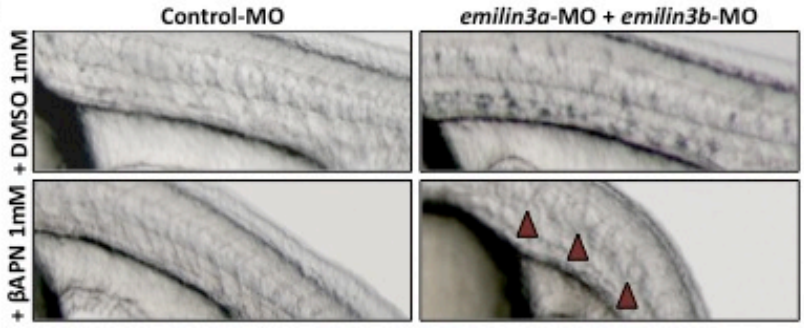

C

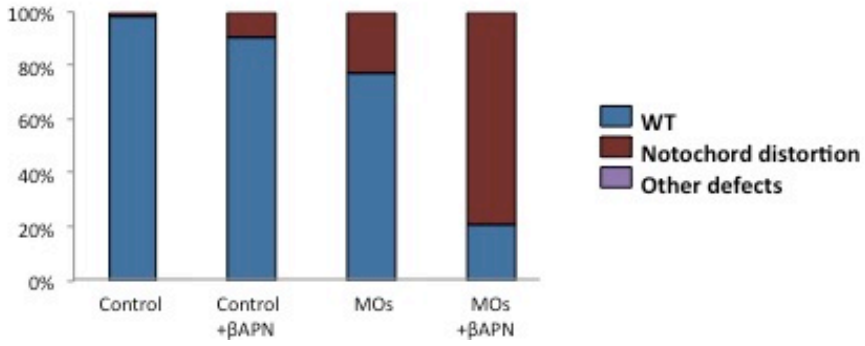

FIGURE 23. Characterization of the muscle phenotype of Emilin-3 morphant embryos. Toluidine blue semithin sections from the trunk region of 30 hpf *emilin3a/3b* double morphant zebrafish embryos show somite disorganization and presence of some vacuolated cells in the medial region of somites in close contact with the notochord basement membrane (arrows in **A**) where slow muscle cells differentiation takes place. Embryos injected with control morpholinos have a normal morphology. Staining with Phalloidin-FITC at 48 hpf show wavy appearance of muscles in *emilin3a/3b* morphant embryos (**B**). Staining for the fast myosin heavy chain-1 show no differencies at 24 hpf indicating that differentiation of fast muscle cells is not affected by Emilin-3 knockdown (**C**). cv, caudal vein; da, dorsal aorta; no, notochord; nt, neural tube; lo, lateral organ; so, somite. Scale bar: 50 μm

FIGURE 23

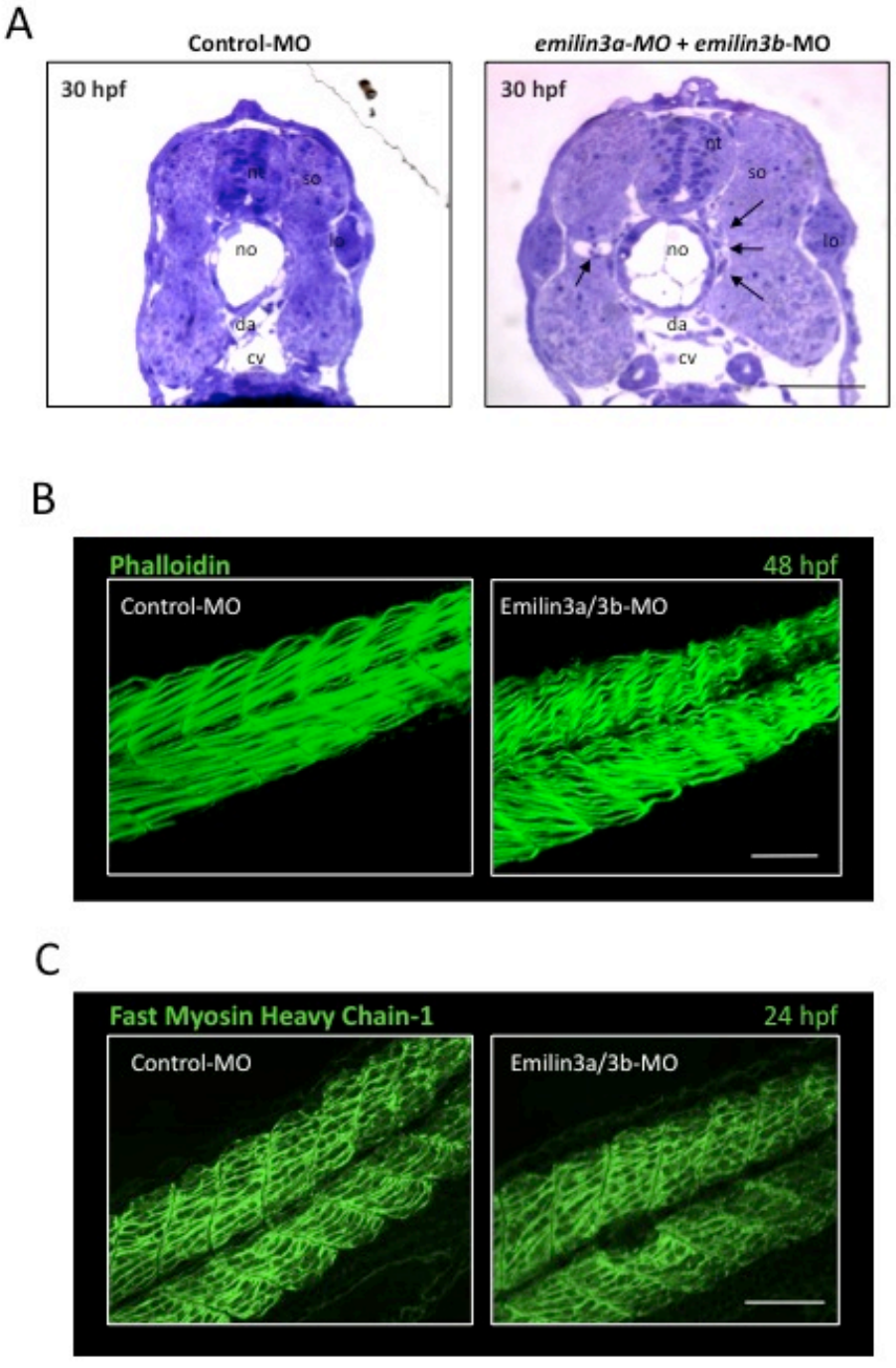
A
Control-MO
emilin3a-MO + emilin3b-MO
30 hpf
30 hpf
nt
so
no
lo
da
cv
B
Phalloidin
48 hpf
Control-MO
Emilin3a/3b-MO
C
Fast Myosin Heavy Chain-1
24 hpf
Control-MO
Emilin3a/3b-MO

FIGURE 24

A

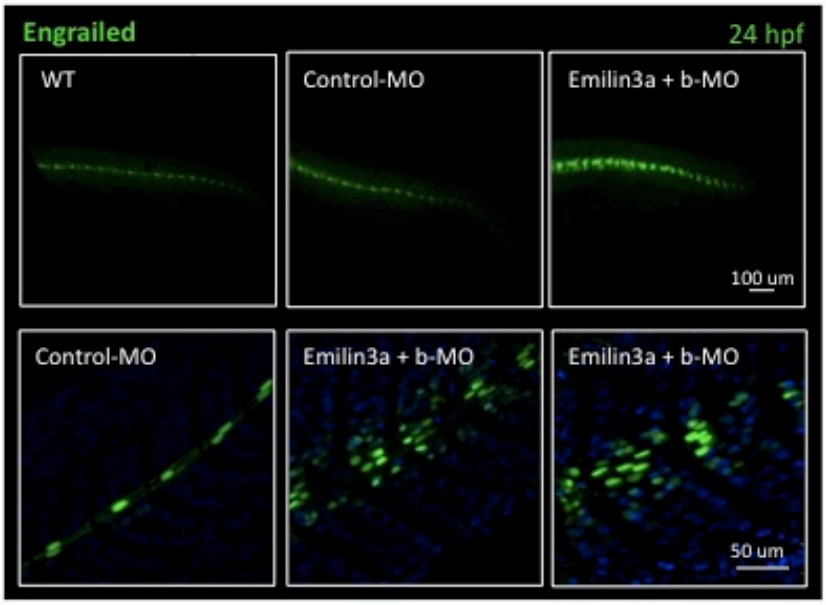

B

	Trunk pioneers	Trunk MMFs	Tail pioneers
Control-MO (n=4,x=5)	1-4	2-18	0-2
Emilin3a/3b-MO (n=5,x=5)	2-8*	12-29*	1-5*

FIGURE 24. Engrailed positive cells are increased in morphant embryos. Lateral view of 24 hpf embryos. To assess whether Emilin-3 deficiency could influence adaxial cell commitment selectively in slow muscle myofibers, control and *emilin3a/3b* morphant zebrafish embryos were stained for the Engrailed transcription factor that marks muscle pioneers and medial fast fibers (**A**). Quantification of muscle pioneers and medial fast fibers (MFF) nuclei in the trunk and tail region of control and morphant embryos. Both cell types are significantly increased in *emilin3a/3b* morphants, suggesting a differentiation unbalance of adaxial cells (**B**). WT, wild-type. n, the number of embryos counted; x, the numer of somites counted per embryo. Asterisks indicate values that are significantly different (P=0.01) from the control value.